



**HAL**  
open science

## Solvent extraction in non-ideal eutectic solvents – Application towards lanthanide separation

Ueslei G Favero, Nicolas Schaeffer, Helena Passos, Kaíque a M L Cruz, Duarte Ananias, Sandrine Dourdain, Maria C Hespanhol

### ► To cite this version:

Ueslei G Favero, Nicolas Schaeffer, Helena Passos, Kaíque a M L Cruz, Duarte Ananias, et al.. Solvent extraction in non-ideal eutectic solvents – Application towards lanthanide separation. Separation and Purification Technology, 2023, 314, pp.123592. 10.1016/j.seppur.2023.123592 . hal-04593949

**HAL Id: hal-04593949**

**<https://hal.science/hal-04593949v1>**

Submitted on 30 May 2024

**HAL** is a multi-disciplinary open access archive for the deposit and dissemination of scientific research documents, whether they are published or not. The documents may come from teaching and research institutions in France or abroad, or from public or private research centers.

L'archive ouverte pluridisciplinaire **HAL**, est destinée au dépôt et à la diffusion de documents scientifiques de niveau recherche, publiés ou non, émanant des établissements d'enseignement et de recherche français ou étrangers, des laboratoires publics ou privés.



Distributed under a Creative Commons Attribution - NonCommercial - NoDerivatives 4.0  
International License



## Solvent extraction in non-ideal eutectic solvents – Application towards lanthanide separation

Ueslei G. Favero<sup>a</sup>, Nicolas Schaeffer<sup>b,\*</sup>, Helena Passos<sup>b</sup>, Kaíque A.M.L. Cruz<sup>a</sup>, Duarte Ananias<sup>b</sup>, Sandrine Dourdain<sup>c</sup>, Maria C. Hespanhol<sup>a,\*</sup>

<sup>a</sup> Group of Analysis and Education for Sustainability (GAES), Chemistry Department, Federal University of Viçosa (UFV), Viçosa, MG 36570–900, Brazil

<sup>b</sup> CICECO - Aveiro Institute of Materials, Department of Chemistry, University of Aveiro, 3810-193 Aveiro, Portugal

<sup>c</sup> Institut de Chimie Séparative de Marcoule, ICSM, CEA, CNRS, ENSCM, Univ Montpellier, BP 17171, Marcoule, 30207 Bagnols-sur-Cèze, France

### ARTICLE INFO

#### Keywords:

Deep eutectic solvents  
Type V eutectic  
Solvent extraction  
Hydrogen bonding  
Small angle X-ray scattering

### ABSTRACT

Hydrophobic eutectic solvents (HES) emerged as promising substitutes to the conventional organic phase used in the solvent extraction (SX) of metal ions due to the avoidance of diluents and the suppression of third-phase manifestation. However, HES present a highly structured liquid phase defined by hydrogen-bonded interactions such that intercomponent interactions are expected to play a greater role in SX using HES compared to a diluted extractant solution. In this work, the extraction of lanthanides from nitrate media by the non-ideal solvent composed of decanoic acid (C<sub>10</sub>OOH) and trioctylphosphine oxide (TOPO) was determined as a function of the lanthanide cation selection, HES molar fraction, HNO<sub>3</sub> concentration, and temperature. Through the systematic variation of these parameters, the delicate balance between complexation and solvent reorganisation and its influence on the extraction and metal selectivity is determined by metal partition experiments, time resolved fluorescence and Raman spectroscopy, and small-angle X-ray scattering (SAXS). A compromise between maximum Ln<sup>3+</sup> loading and selectivity was observed, driven by the variation in the quantity of weakly H-bonded TOPO and the change in the configurational entropy of the mixture. All results point towards the need to explicitly consider the HES phase structuration and its compositional changes with solute co-extraction on the Ln<sup>3+</sup> extraction as no change in the extracted complex speciation was observed across all tested conditions. The C<sub>10</sub>OOH + TOPO was used as a model system due as lanthanide extraction using TOPO and carboxylic extractants is well described whilst the phase diagram and properties of the eutectic are reported. Nevertheless, the derived conclusions are translatable to other systems and can help guide the design and application of possible HES combinations for SX.

### 1. Introduction

Sustainable metallurgy stands uniquely poised to reduce the environmental impact of primary ore extraction whilst providing new avenues for the metallic value recovery from secondary “urban ores” including the rapidly growing electronic waste, thereby closing the loop [1–2]. Of the various metallurgical options, hydrometallurgy is hailed as the environmentally friendly alternative to the industrially preferred pyrometallurgical option due to its ability to recover metals from low-grade matrices, gentler process conditions and greater flexibility, solvent regeneration and limited gaseous emissions [3]. The hydrometallurgical process is divided in three major steps: leaching, separation and refining. Solvent extraction (SX) represents the major industrial mean to

separate and purify many metal ions including copper, zinc, platinum group metals, uranium or lanthanides from complex leachates through their transfer from an aqueous to an immiscible organic phase [4,5]. This is typically achieved by means of amphiphilic molecules, named extractants, with a chelating polar group to ensure metal coordination and an apolar part stabilising the resulting complex in the organic phase. However, complex process flowsheet arising from the poor separation selectivity between similar elements results in the use of significant volumes of corrosive effluents and hazardous organic solvents and limits the wider applicability of SX.

For example, the stable oxidation state of +3 and near-identical chemistries of trivalent lanthanide cations (Ln<sup>3+</sup>) renders their mutual separation both technologically and environmentally challenging [6–7].

\* Corresponding authors.

E-mail addresses: [nicolas.schaeffer@ua.pt](mailto:nicolas.schaeffer@ua.pt) (N. Schaeffer), [mariacarmo@ufv.br](mailto:mariacarmo@ufv.br) (M.C. Hespanhol).

<https://doi.org/10.1016/j.seppur.2023.123592>

Received 27 January 2023; Received in revised form 1 March 2023; Accepted 10 March 2023

Available online 15 March 2023

1383-5866/© 2023 The Author(s). Published by Elsevier B.V. This is an open access article under the CC BY-NC-ND license (<http://creativecommons.org/licenses/by-nc-nd/4.0/>).

The shielded nature of the 4f Ln valence electrons makes the interactions with ligands electrostatic (rather than covalent) in nature, with the coordination numbers and complex geometries determined mainly by steric factors [8]. In the absence of redox accessible pairs in aqueous media for most Ln<sup>3+</sup>, SX separation relies on the small monotonic changes in the properties brought about by poor 4f electrons shielding and the gradual decrease of the ionic radius along the series from La<sup>3+</sup> to Lu<sup>3+</sup>, also known as the lanthanide contraction. The thermodynamic similarity of Ln<sup>3+</sup> leads to small changes of less than 6.5 kJ mol<sup>-1</sup> in binding affinities between adjacent cations [9]. The almost linear evolution of the stability constants, irrespective of the ligand nature [9–12], attests to the difficulty in achieving a selective extraction of neighbouring pairs based on speciation alone. The fundamental chemistry problem behind Ln<sup>3+</sup> separation is one of global importance. The mutual separation of Ln<sup>3+</sup>, identified as one of the key separation challenges of the 21st century [6], occurs over approximately dozens of counter-current extraction stages and is conservatively estimated to account for 30 % of the total associated environmental impacts of Ln<sup>3+</sup> oxide production [5,13]. This generates substantial volumes of volatile and potentially toxic organic effluents due to relatively dilute operating conditions applied, from ppm levels to approximately 15 g L<sup>-1</sup> of target solute.

In this context, the development of advanced functional solvents presenting increased efficacy with decreased environmental impacts is highly relevant. Hydrophobic eutectic solvents (HES) emerged as promising substitutes for the traditional apolar phase in SX [14]. HES are low-melting binary mixtures that present interesting properties due to the liquefaction and enhanced solubility provided by the decrease of the melting point of the mixture when compared to those of the starting pure constituents [15]. Extractant molecules can be incorporated as one of the two components of a eutectic systems, acting both as the apolar phase former and chelating agent thereby allowing for greater extractant concentrations and more intensive separation processes. This was successfully demonstrated for the extraction of uranyl, platinum group metals, transition metals, boron or lithium [16–23]. To the best of our knowledge, only one work systematically studied the partition of Ln<sup>3+</sup> in a ternary HES of 1-decanol:oleic acid:bis(2-ethylhexyl) amine [24]. The suppressed Y<sup>3+</sup> extraction resulted in an improved separation of the heavier Ln<sup>3+</sup> whilst the loaded HES could be easily stripped reused over multiple SX cycles. Through judicious selection of the hydrophobic components, which can include cheap natural products such as terpenoids, fatty acids and/or alcohols [15], HES avoid the use of organic diluents whilst presenting negligible water solubilities and viscosities associated with ionic solvents for SX. Furthermore, HES present the added advantage that no new compounds are synthesised, relying solely on the molar ratio of the components thereby simplifying the economical, toxicological, and environmental assessment.

First coined in 2003 [25], the prefix *deep* is assigned for eutectic mixtures for which the eutectic point temperature should be lower to that of an ideal liquid mixture [15]. The increased melting point depression stems from the stronger intermolecular interactions between the eutectic components relative to those present in the pure compounds [14,26]. Relating this “deepness” to SX, there is growing evidence that metal extraction in strongly non-ideal HES [27–28] proceeds differently to that in ideal or quasi-ideal systems [29]. The free energy of transfer for a given electrolyte in SX can be decomposed into three main contributions, namely (i) the favourable complexation energy of the metal ion and extractant, which is partially quenched by (ii) solute confinement in the highly concentrated polar domains of the organise phase and (iii) solvent-phase nano-structure reorganization around the extracted and coextracted species ( $\Delta G_{\text{Structuration}}$ ) [30–31]. Compared to conventional SX in which the organic phase structuration is often a consequence of metal ions and polar solute extraction, [32] mixed extractant interactions [33–34] as well as diluent effects [35] are expected to be more important when using HES due to the intrinsic nature of the solvent. HES presenting negative thermodynamic deviations from ideality

yield highly structured liquid phase defined by intermolecular interactions [36]. These solvents are characterised by hydrogen bonding (H-bonding) to yield sterically crowded pre-organised phases, the nature of the latter depending on the selection of the hydrogen bond donor (HBD) and acceptor (HBA) components and their respective molar ratio. The organisation of DES translates into the presence of structural heterogeneity and the formation of defined polar domains as shown for the thymol + menthol system by small-angle X-ray scattering analysis (SAXS) [36].

Pre-organisation of the solvent phase is in some cases viewed as undesirable due to the potential for an antagonistic extraction mechanism [37]. Comparatively, less attention has been paid to the possibility of tuning the selectivity by controlling the dynamics and mesoscale organisation of a “concentrated” SX organic phase [32,38]. The control of the intermolecular interactions dictating the hierarchical self-assemblies in SX, and therefore the magnitude of the  $\Delta G_{\text{Structuration}}$  contribution, affords a new avenue for the design of next-generation separation techniques. As structured solvent phases in SX are in dynamic equilibrium, considering only the first solvation sphere of the extracted ions provides a limited assessment of the SX free-energy landscape and does not fully exploit the potential stabilising forces over longer correlation lengths, such as second neighbour and percolation effects. H-bonding in the “soft” outer-sphere of “hard” metal–ligand complexes with non-ionic extractants plays a critical role in determining the selectivity of lanthanide separation [39–40]. Additionally, the abundant presence of H-bonds in the apolar phase of SX was shown to swell the polar network volume, yielding an increase in the extraction efficiency of metal ions that are solubilised but non-chelated (i.e. no modification of the actual metal–ligand complexation energy) [41–43]. Finally, H-bond donors are commonly added as phase modifiers to prevent the critical phenomenon of third-phase formation in which the apolar phase splits into a heavy and light phase upon extraction of polar solutes above a certain concentration [44]. An analysis of these effects upon metal extraction in HES merits further investigation and could be of interest for difficult separation that typically rely on small variations of complexation energies.

In this work, the SX of selected light, middle and heavy lanthanides from nitric acid media is studied in the H-bonded assembly that is the deep HES of trioctylphosphine oxide (TOPO) and decanoic acid (C<sub>10</sub>OOH). The choice of potential HES combinations is restricted by the chemical stability of the hydrogen bond donor in the presence of the strongly oxidising HNO<sub>3</sub> acid, such that most phenolic and alcohol compounds are excluded. The TOPO + C<sub>10</sub>OOH phase diagram was previously reported and shows strong negative deviations to ideality manifested by a melting point depression of 29.2 K below that predicted for an ideal system and a large liquidus composition (at 298 K) spanning a TOPO molar fraction ( $x_{\text{TOPO}}$ ) range of 0.10 to 0.55 [18]. Furthermore, lanthanide extraction using TOPO and the equivalent Cyanex 923 is well described, [45–47] facilitating the comparison between SX in the studied HES and conventional diluents. Through the systematic variation of metal cation type,  $x_{\text{TOPO}}$ , and HNO<sub>3</sub> concentration, the delicate balance between complexation and solvent reorganisation and its influence on the extraction and metal selectivity is determined. The obtained trends can expand and guide the design and application of possible HES combinations based on well-known non-ionic lanthanide ligands such as phosphate, diglycolamide or malonamide-type extractants.

## 2. Experimental

### 2.1. Reagents

Trioctylphosphonine oxide (TOPO) (99 %), thymol (99–101 %), decanoic acid (99 %) (C<sub>10</sub>OOH), nickel nitrate hexahydrate (>98.5 %), neodymium nitrate hexahydrate (99.9 %), praseodymium nitrate hexahydrate (99.99 %), yttrium nitrate hexahydrate (99 %), lanthanum nitrate hexahydrate (99.99 %), and cerium (III) nitrate hexahydrate

(99.99 %) were obtained from Sigma Aldrich (USA). Iron chloride (III) hexahydrate (98 %), sodium nitrate (99 %), and nitric acid 65 % were obtained from Vetec (Brazil). Solutions of  $Ce^{4+}$  (9.585 mg g<sup>-1</sup>),  $Eu^{3+}$  (9.577 mg g<sup>-1</sup>),  $Gd^{3+}$  (9.683 mg g<sup>-1</sup>) and  $Lu^{3+}$  (9.683 mg g<sup>-1</sup>) were obtained from Specsol (Brazil). Trioctylamine (TOA, 98 %) was obtained from Fluka (USA).

## 2.2. Solute partition

The partition of metal ions [ $La^{3+}$ ,  $Ce^{3+}$ ,  $Ce^{4+}$ ,  $Pr^{3+}$ ,  $Nd^{3+}$ ,  $Eu^{3+}$ ,  $Gd^{3+}$ ,  $Y^{3+}$ , and  $Lu^{3+}$ ] was performed in a two-phase liquid system formed by the mixture of 0.50 g of HES  $C_{10}OOH$  + TOPO (molar fraction of TOPO of either 0.3, 0.4 or 0.5) with 1.0 g aqueous solution of  $HNO_3$  (from 0.10 to 6.0 mol L<sup>-1</sup>) or 2.0 mol L<sup>-1</sup> of  $NaNO_3$ . A constant individual metal ion concentration of 7.5 mmol kg<sup>-1</sup> was used throughout. Additionally, the partition of  $Eu^{3+}$  and  $Lu^{3+}$  was studied as a function of temperature from 293 to 343 K for two  $HNO_3$  concentrations (1.0 and 6.0 mol L<sup>-1</sup>) and three  $x_{TOPO}$  (0.3 to 0.5). The mixture of HES and aqueous solution was always performed under agitation of 1 min and the separation of phases accelerated by centrifugation at 10000 rpm for 5 min. The metal content in the aqueous phase before and after extraction was analyzed via Microwave Plasma Atomic Emission Spectroscopy (MP-AES, Agilent Technologies, USA). The partition of  $HNO_3$  under the same extraction conditions in the absence of metal cations was determined by UV-Vis analysis of the aqueous phase (Shimadzu, UV-2550, TCC-240, Japan) through the absorbance peak at 301 nm (calibration curve determined from 0.1 to 0.8 mol L<sup>-1</sup>) using a quartz cell with a path length of 1 cm. The water content in the HES phase following extraction was measured using a coulometric Karl Fischer titrator (Metrohm 831, Switzerland) with an Hydranal® solution from Sigma-Aldrich. Due to the incompatibility of the  $HNO_3$  with the titrating solution, the organic phase was first neutralised using TOA prior to titration following a reported methodology as the resulting [TOAH][ $NO_3$ ] is soluble in the HES [48]. An excess of TOA (0.1 g) was added to 0.5 g of the HES sample and agitated at 298 K for 1 h prior to measurement. The water content of the sample was corrected considering the water content of pure TOA that was independently measured.

## 2.3. Luminescence measurements

The emission and excitation spectra were recorded at ambient-temperature using a Fluorolog®-3Horiba Scientific (Model FL3-2 T) spectroscope. with a modular double grating excitation spectrometer (fitted with a 1200 grooves/mm grating blazed at 330 nm) and a TRIAX 320 single emission monochromator (fitted with a 1200 grooves/mm grating blazed at 500 nm; reciprocal linear density of 2.6 nm mm<sup>-1</sup>) coupled to a R928 Hamamatsu photomultiplier. using the front face acquisition mode. The excitation source was a 450 W Xe arc lamp. The emission spectra were corrected for detection and optical spectral response of the spectrofluorimeter and the excitation spectra were corrected for the spectral distribution of the lamp intensity using a photodiode reference detector. Time-resolved measurements have been carried out using a 1934D3 phosphorimeter coupled to the Fluorolog®-3. and a Xe-Hg flash lamp (6 μs/pulse half width and 20–30 μs tail) was used as the excitation source.

## 2.4. Raman spectroscopy

Raman spectra were acquired on a Bruker MultiRAM equipped with a 1064 nm Nd-YAG laser source and a nitrogen cooled germanium detector. All spectra were recorded in the 3600 to 100 cm<sup>-1</sup> range with a resolution of 4 cm<sup>-1</sup>. A total of 500 scans and a laser power of 350 mW and was applied. The obtained spectra were deconvoluted using the Origin software package. The baseline was fitted using an exponential decay function and subtracted. The resulting area was deconvoluted into Lorentzian components.

## 2.5. Small-angle X-ray scattering (SAXS) measurements

SAXS experiments were performed using a home-built SAXS camera at the Institut de Chimie Séparative de Marcoule (ICSM). The setup involves a molybdenum source delivering a 1 mm circular beam of energy at 17.4 keV. A monochromatic beam was obtained by using a Fox-2D multishell mirror, and collimation of the beam was achieved using 2 sets of “scatterless” slits, which are crucial for the quantification of weak scattering near the beam-stop, together with precise monitoring of the transmission of the sample and solvents used as the reference. The scattering pattern was recorded using a MAR345 two-dimensional imaging plate, with a typical duration of 1 h. The measurements were performed in transmission geometry using 2 mm glass capillaries. The experimental resolution was set to  $\Delta q/q = 0.05$ . The detector count was normalised to the differential cross-section per unit volume (in cm<sup>-1</sup>) with either a 2.36 mm thick high-density polyethylene sample (from Goodfellow®) ( $I_{max} = 5.9$  cm<sup>-1</sup>) or 3 mm water for which the level of scattering at low  $q$  is known ( $1.64 \times 10^{-2}$  cm<sup>-1</sup>). Data pre-analysis was performed using PYSAXS software, considering the electronic background of the detector (where the flat-field response was homogeneous), transmission measurements (using a photodiode that can be inserted upstream of the sample), and empty cell subtraction. The scattering intensities are expressed as a function of the magnitude of the scattering vector.

## 3. Results and discussion

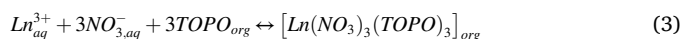
### 3.1. SX in TOPO + $C_{10}OOH$ – general considerations

In SX, the extraction strength for a given lanthanide ion ( $Ln^{n+}$ ) is expressed as the distribution ratio ( $D_{Ln}$ ) shown in equation (1) whilst the selectivity reflects the affinity of the system for one  $Ln^{n+}$  cation over another and is expressed by the separation factor ( $SF$ ) in equation (2).

$$D_{Ln} = \frac{[Ln]_{HES}}{[Ln]_{aq}} \quad (1)$$

$$SF_{Ln1/Ln2} = \frac{D_{Ln1}}{D_{Ln2}} \quad (2)$$

where “HES” and “aq” indicate the concentration of Ln in the HES and aqueous phase respectively. In non-ionic systems,  $D_{Ln}$  and  $SF$  depend not only on the capacity of the organic phase to accommodate the ionic lanthanide species but also the nature and concentration of the accompanying counter-ions to ensure charge neutrality. The extraction mechanism for  $Ln^{3+}$  using 0.2 mol L<sup>-1</sup> TOPO diluted in toluene (not considering water molecules) was previously determined based on slope analysis as [46,49]:



Whilst slope analysis regression is possible for systems that can be described using a simple set of equilibria, this approach does not properly describe complex extraction mechanisms with multiple equilibria as can occur in the case of mixtures such as HES [30]. In the latter, as TOPO is both the chelating agent and one of the eutectic phase former, the ratio between the concentration of free extractants for SX and the total concentration in the system is blurred. An additional consideration is the role of  $C_{10}OOH$  on the distribution as carboxylic acid-based extractants such as Versatic 10 are known as lanthanide extractants [50]. Throughout this work, the systematic variation of the HES phase composition is represented by the change in the TOPO molar fraction  $x_{TOPO}$ . However, as  $x_{TOPO} = 1 - x_{C_{10}OOH}$  in the HES phase, such variations in composition also address the role of  $C_{10}OOH$  on the extraction and liquid phase organisation. To simplify the system interpretation, reduce emulsification and loss of the HES component to the aqueous phase, extraction was investigated for aqueous phase acidities below the

pKa (~4.9) of  $C_{10}OOH$ . Under such conditions, carboxylic-based extractants are not reported to extract lanthanide [50]. Nevertheless,  $C_{10}OOH$  can interact with TOPO as well as stabilise co-extracted nitrate anions and molecular nitric acid thereby indirectly contributing to  $Ln^{3+}$  extraction. Considering these limitations, no effort was made to rationalise the obtained  $D_{Ln}$  through slope analysis. Rather,  $D_{Ln}$  values were used to determine the Gibbs free energy of transfer of a metal ion ( $\Delta G_R$ ) given by equation (4) as there is no assumption of a dominant supra-molecular extraction equilibrium that would consider all other species present in the solution [51].

$$\Delta G_R = -RT \ln(D_{Ln}) \quad (4)$$

In equation (4), the reaction Gibbs energy of the transfer standard state is defined for a solvent containing all the species but lanthanide salt. It is therefore the free energy per mole of the transferred species and not the raw difference of a given sample versus a reference state, as classically noted  $\Delta G^0$  in thermodynamics.

### 3.2. SX in TOPO + $C_{10}OOH$ – Influence of $HNO_3$ concentration

In a first instance, the influence of the aqueous  $HNO_3$  concentration from 0.1 to 6.0 mol  $L^{-1}$  on the extraction of  $La^{3+}$ ,  $Ce^{3+}$ ,  $Pr^{3+}$ ,  $Nd^{3+}$ ,  $Eu^{3+}$ ,  $Gd^{3+}$ ,  $Y^{3+}$  and  $Lu^{3+}$  by the  $C_{10}OOH$  + TOPO HES was determined and presented in Fig. 1A.  $Y^{3+}$  was used as a proxy for  $Ho^{3+}$  due to their similar ionic radii and are discussed interchangeably in the rest of this work. A constant metal concentration of 7.5 mmol  $L^{-1}$ , organic to aqueous phase ratio (O/A) of 0.5,  $T = 298$  K, and TOPO molar fraction of 0.5 were applied. All reported  $D_{Ln}$  values are available in Table S1–S4 of

the ESI. It is important to note that (i) no third-phase formation was observed and (ii) no loss of the HES component to the aqueous phase after extraction was detected by  $^1H$  NMR (detection limit of 5 mol.%) for any of the extractions performed.

As shown in Fig. 1A, the distribution ratios irrespective of the lanthanide ion present a maximum for  $0.5 \leq [HNO_3] \leq 1.0$  mol  $L^{-1}$  and decrease thereafter with increasing  $[HNO_3]$ . The speciation of trivalent lanthanides for the studied  $HNO_3$  range does not significantly vary, with the  $[Ln(H_2O)_n]^{3+}$  ( $n = 8$  or  $9$ ) and  $[Ln(NO_3)(H_2O)_{n-1}]^{2+}$  reported to be the dominant aqueous phase complexes at the lowest and highest  $HNO_3$  concentration investigated respectively [53–54]. By ruling out the influence of speciation, the decrease of  $D_{Ln}$  is attributed to the competitive co-extraction of  $HNO_3$  (*infra vide*) [55–57].  $HNO_3$  is a fairly weak inorganic acid and its protonated and dissociated form exist in equilibrium above 3.0 mol  $L^{-1}$ , [58] with the equilibrium shifted towards the protonated specie in lower-dielectric media [59]. Plotting  $\Delta G_R$  as a function of the initial aqueous  $HNO_3$  concentration for one light, middle and heavy lanthanide (Fig. 1B) clearly identifies two extraction regimes in which  $\Delta G_R$  varies monotonically. The first regime is dominated by  $Ln^{3+} \bullet TOPO$  complexation for  $[HNO_3] \leq 1.0$  mol  $L^{-1}$  whilst the second is influenced by the HES phase re-organization induced by acid co-extraction for  $[HNO_3] \geq 1.0$  mol  $L^{-1}$  as will be demonstrated further on. No inferences are made as to the extraction mechanism and stoichiometry of the metal-extractant chelate in these two regimes and if these differ at all.

The shift between extraction regimes not only changes the distribution ratio for a given lanthanide but also varies the  $D_{Ln}$  trend along the Ln series. This is exemplified in Fig. 1C by plotting the  $D_{Ln}$  obtained for a

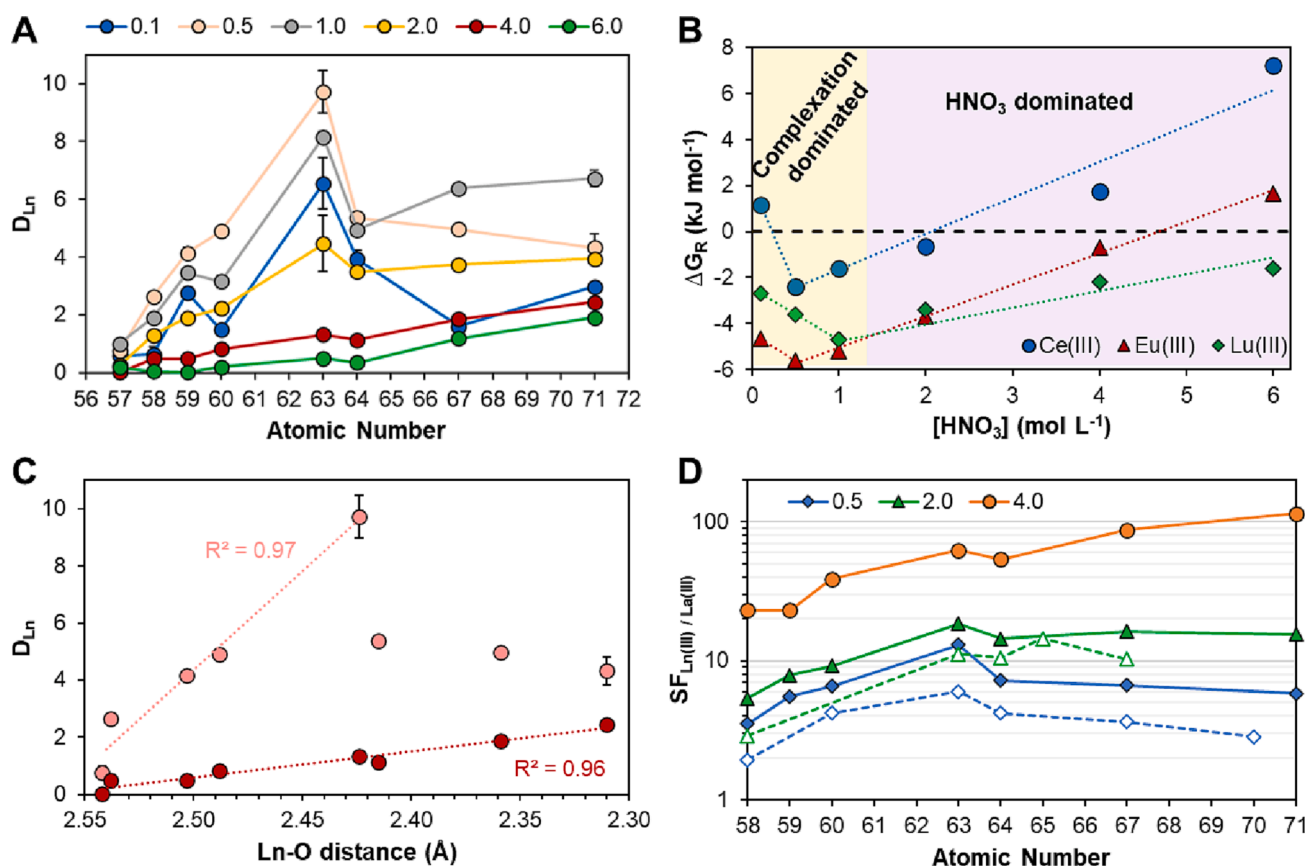


**Fig. 1.** A) Distribution coefficients ( $D_{Ln}$ ) and B) Gibbs free energies of transfer of  $Ln^{3+}$  in the  $C_{10}OOH$  + TOPO HES as a function of the initial aqueous phase  $HNO_3$  concentration ( $O/A = 0.5$ ,  $x_{TOPO} = 0.5$ ,  $[Ln^{3+}] = 7.5$  mmol  $L^{-1}$ ). C)  $D_{Ln}$  as a function of the ionic radii of trivalent lanthanide cations (taken from ref<sup>52</sup>) for two  $HNO_3$  concentration of 0.5 and 4.0 mol  $L^{-1}$ . D) Separation factors for  $Ln^{3+}/La^{3+}$  pairs in the  $C_{10}OOH$  + TOPO HES for a fixed  $HNO_3$  concentration of 0.5, 2.0 and 4.0 mol  $L^{-1}$  (full lines) and compared against traditional SX using TOPO at the same  $HNO_3$  concentration (dashed lines) taken from refs [46–47]. Lines are drawn to help the eye. In all cases  $Y^{3+}$  is used as a proxy for  $Ho^{3+}$ .

fixed  $\text{HNO}_3$  concentration of 0.5 and 4.0 mol L<sup>-1</sup> against the ionic radii of trivalent Ln<sup>3+</sup> cations [52]. At lower  $\text{HNO}_3$  concentrations, the  $D_{\text{Ln}}$  suggest a tetrad effect [60] and present two clear groupings. An initial rise in  $D_{\text{Ln}}$  is observed with the increasing charge density of the Ln cation, reaching a maximum for Eu<sup>3+</sup>, followed by a sharp decrease from Eu<sup>3+</sup> to Gd<sup>3+</sup> and further reductions in  $D_{\text{Ln}}$  for heavier Ln. A similar maximum  $D_{\text{Ln}}$  range from Eu<sup>3+</sup> to Tb<sup>3+</sup> (depending on the study) was observed for TOPO in conventional organic diluents for a  $\text{HNO}_3$  concentration of 0.5 mol L<sup>-1</sup> [46–47]. A notable difference upon inclusion of TOPO in HES is the sharp break in  $D_{\text{Ln}}$  between the adjacent Eu<sup>3+</sup> and Gd<sup>3+</sup>, which was not observed in the conventional SX, yielding an interesting  $\text{SF}_{\text{Eu}/\text{Gd}}$  of 1.81 at this acid concentration. Although no clear “gadolinium break” was observed in the coordination number of hydrated lanthanides, [61] Gd<sup>3+</sup> is often considered as a transition point between the nine-coordinate structure preferred by the lighter lanthanides and the eight-coordinate structure of the heavier Ln [61–62]. The break in  $D_{\text{Ln}}$  with decreasing ionic radius after Eu<sup>3+</sup> is therefore assigned to steric hindrances to coordination by bulky TOPO ligands imposed by the change in Ln<sup>3+</sup> coordination number and further exacerbated by the sterically crowded nature of the HES phase. This is consistent with the variation in the coordination number of Ln<sup>3+</sup> nitrate complexes with triethylphosphine oxides (Et<sub>3</sub>PO) from Ln(NO<sub>3</sub>)<sub>3</sub>(Et<sub>3</sub>PO)<sub>3</sub> for the lighter lanthanides to mixtures of Ln(NO<sub>3</sub>)<sub>3</sub>(Et<sub>3</sub>PO)<sub>3</sub> and Ln(NO<sub>3</sub>)<sub>3</sub>(Et<sub>3</sub>PO)<sub>2</sub> for the heavier metals as determined from single crystal X-ray crystallography [49,63]. In fact, the apparent equilibrium constant for Ln<sup>3+</sup> extraction from nitrate media using phosphine oxide extractants presenting a lesser steric restriction is found to increase with decreasing ionic radii as shown in Figure S1 and in contrast to the results in Fig. 1A, further confirming the influence of the complex geometry on the measured  $D_{\text{Ln}}$ .

Raising the initial aqueous  $\text{HNO}_3$  concentration to 4.0 mol L<sup>-1</sup> suppresses the extraction of the lighter Ln<sup>3+</sup> relative to the heavier ones and eliminates the break in  $D_{\text{Ln}}$  at Eu<sup>3+</sup>, resulting in the linear increase of  $D_{\text{Ln}}$  with decreasing ionic radius as shown in Fig. 1C. The change in extraction regime from an “complexation dominated” one to “ $\text{HNO}_3$  dominated” is reflected in the  $D_{\text{Ln}}$  trends, as shown in Fig. 1B–C, and by extension in the derived separation factors. The SFs between Ln<sup>3+</sup> and La<sup>3+</sup> as reference for three initial  $\text{HNO}_3$  concentrations of 0.5, 2.0 and 4.0 mol L<sup>-1</sup> are presented in Fig. 1D and compared, when available, with reported SX data for TOPO in organic diluents at the same acid concentration [46–47]. Similar trends in the  $\text{SF}(\text{Ln}^{3+}/\text{La}^{3+})$  between SX in HES and in conventional system for 0.5 and 2.0 mol L<sup>-1</sup>  $\text{HNO}_3$  are obtained albeit with increased SFs in HES due to the consistently poor partition of La<sup>3+</sup> across all tested acid concentrations. This confirms that non-ionic extractants can be incorporated as HES constituents without losing their extraction characteristics. Under mildly acidic conditions, a maximal SF is obtained for the Eu/La pair in HES media with  $\text{SF}_{\text{Eu}/\text{La}} = 13.0$  and 18.4 for 0.5 and 2.0 mol L<sup>-1</sup>  $\text{HNO}_3$  respectively. However, for  $[\text{HNO}_3] \geq 4.0$  mol L<sup>-1</sup> a change in the selectivity is observed, permitting the efficient separation of heavy from light Ln<sup>3+</sup> with a  $\text{SF}_{\text{Lu}/\text{La}} = 114.7$  at 4.0 mol L<sup>-1</sup>  $\text{HNO}_3$ . The observed tendencies are similar to that for tributyl phosphate (TBP) extractant in which a maximum extraction is obtained for Gd<sup>3+</sup> at  $\text{HNO}_3$  concentrations below 4.0 mol L<sup>-1</sup> ( $\text{SF}_{\text{Eu}/\text{La}} \sim 20$ ) but  $D_{\text{Ln}}$  proceeds in an approximately linear manner from light to heavy Ln<sup>3+</sup> at  $\text{HNO}_3$  concentrations above 10.0 mol L<sup>-1</sup> ( $\text{SF}_{\text{Lu}/\text{La}} \sim 100$ ) [64–65]. The obtained  $\text{SF}_{\text{Lu}/\text{La}}$  is comparable to other conventional SX systems using solvating extractants such as Cyanex 923 ( $\text{SF}_{\text{Lu}/\text{La}} = 200$  at  $[\text{NaNO}_3] = 1.0$  mol L<sup>-1</sup> and pH = 3) [66] or *N,N,N',N'*-tetraoctyl diglycolamide (TODGA;  $\text{SF}_{\text{Lu}/\text{La}} = 119$  at  $[\text{HNO}_3] = 1.0$  mol L<sup>-1</sup>) [67] albeit achieved in HES at much higher acid concentrations. Finally, Ln<sup>3+</sup> extraction in nitrate media by TOPO dissolved in “inert” alternative solvents such as non-functionalised fluorinated ionic liquids present improved by variable  $D_{\text{Ln}}$  and resulting SFs values between heavy (Yb<sup>3+</sup>) and light (La<sup>3+</sup>) Ln<sup>3+</sup> from 185 to over 5000. This difference is attributed to the nature of the ionic liquid cation and the extent of its cation-exchange with Ln<sup>3+</sup>, implying a partial loss of the ionic liquid

constituents to the aqueous phase with use. Furthermore, extraction was suppressed for pH values below 1, limiting its applicability under acidic conditions [68].

The possibility to alter the  $D_{\text{Ln}}$  trend in HES by acid co-extraction allows the manipulation of weak interactions (i.e. non-electrostatic) to tune the SFs and achieve a compromise between maximising extraction and enhancing separation for a target lanthanide. To highlight this, substitution of  $\text{HNO}_3$  by 2.0 mol L<sup>-1</sup> NaNO<sub>3</sub>, a stronger salting-out agent that is poorly extracted due to its less favourable Gibbs free energy of hydration, enhances the complexation of the Ln<sup>3+</sup> cations with TOPO. Being not extracted, it is not expected to provoke any restructuring of the HES phase. When using NaNO<sub>3</sub>, close to quantitative extraction of all Ln<sup>3+</sup> was obtained as shown in Fig. 2, resulting in  $D_{\text{Ln}} \gg 100$  for all cations but a decrease in the overall selectivity of the system.

### 3.3. SX in TOPO + C<sub>10</sub>OOH – Influence of TOPO molar fraction

Beyond the aqueous phase acid concentration, another approach to manipulate the HES phase pre-organization is through the variation of the HBD to HBA ratio. Whilst the liquid structure of HES is dynamic in nature, the change in the C<sub>10</sub>OOH to TOPO ratio is expected to vary the energy landscape for the various possible interspecies interactions between the HES constituents and extractable polar species [27]. As such, the influence of HES phase structuration is further investigated through the change in TOPO molar fraction from  $x_{\text{TOPO}} = 0.3$  to 0.5 at two  $\text{HNO}_3$  concentrations of 1.0 and 6.0 mol L<sup>-1</sup> for one light (La<sup>3+</sup>), middle (Eu<sup>3+</sup>) and heavy lanthanide (Lu<sup>3+</sup>). A constant metal concentration of 7.5 mmol L<sup>-1</sup>, O/A = 0.5 and  $T = 298$  K were applied. In addition, the influence of the Ln oxidation state was monitored by following the extraction of Ce<sup>4+</sup> under the same conditions. The obtained distribution factors are shown in Fig. 3A–B and available in Table S3 of the ESI.

A reduction in the  $x_{\text{TOPO}}$  yields a decrease in all  $D_{\text{Ln}}$  although the extent of the relative decrease from  $x_{\text{TOPO}}$  of 0.5 to 0.3 varies with the  $\text{HNO}_3$  concentration as well as the nature of the Ln and its oxidation state. At 1.0 mol L<sup>-1</sup>  $\text{HNO}_3$  (Fig. 3A), extraction of La<sup>3+</sup> is suppressed allowing, for example, to raise the  $\text{SF}_{\text{Lu}/\text{La}}$  from 6.7 to 16.0 as  $x_{\text{TOPO}}$  decreases from 0.5 to 0.4 respectively despite the lower  $D_{\text{Lu}}$  values. No extraction of trivalent lanthanides was observed for  $x_{\text{TOPO}} = 0.3$ . A similar tendency of  $D_{\text{Ln}}$  with  $x_{\text{TOPO}}$  is observed at 6.0 mol L<sup>-1</sup>  $\text{HNO}_3$  (Fig. 3B) for the lighter and middle lanthanides. In contrast,  $D_{\text{Lu}}$  remains comparatively unaffected, yielding in an improved selectivity of the difficult Lu/Eu pair separation from 3.7 to 24.9 as  $x_{\text{TOPO}}$  changes from 0.5 to 0.3 respectively. Contrary to conventional SX in which the

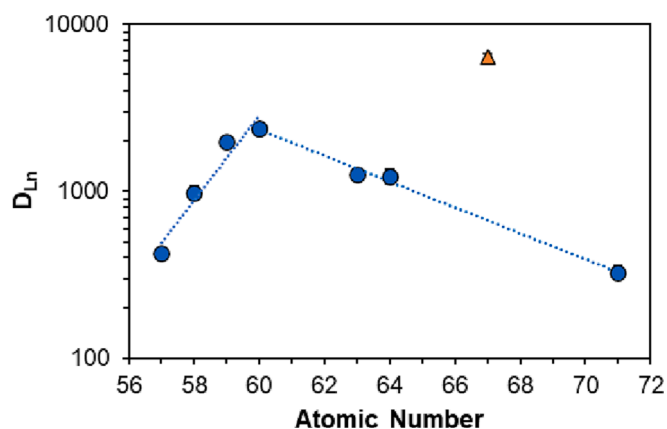


Fig. 2. Distribution coefficients of Ln<sup>3+</sup> in the C<sub>10</sub>OOH + TOPO HES for an initial aqueous phase concentration  $[\text{NaNO}_3] = 2.0$  mol L<sup>-1</sup> (O/A = 0.5,  $x_{\text{TOPO}} = 0.5$ ,  $[\text{Ln}^{3+}] = 7.5$  mmol L<sup>-1</sup>). Lines are drawn to help the eye. Y<sup>3+</sup> is indicated by the orange triangle.  $D_{\text{Ln}}$  values are available in Table S2. (For interpretation of the references to colour in this figure legend, the reader is referred to the web version of this article.)

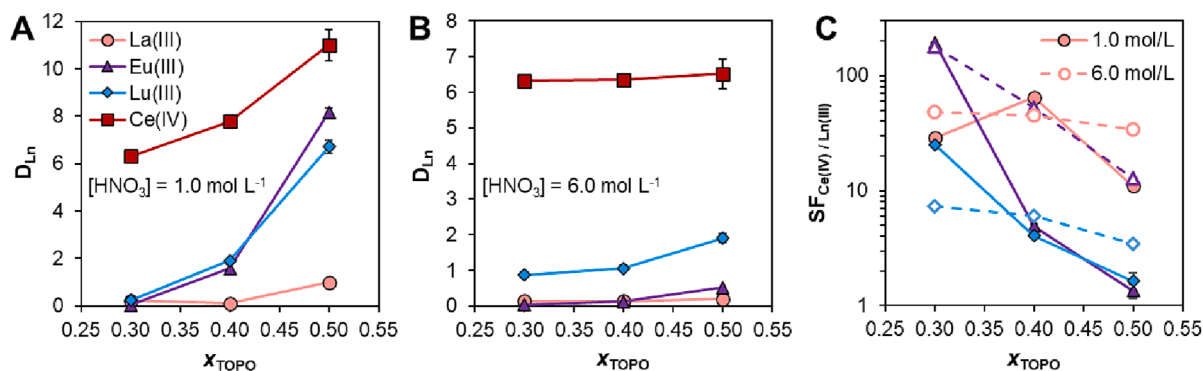


Fig. 3. Lanthanide distribution coefficients in the  $C_{10}OOH + TOPO$  HES as function of the  $x_{TOPO}$  molar fraction for two initial aqueous phase  $HNO_3$  concentrations of A) 1.0 and B) 6.0 mol  $L^{-1}$ . C) Derived  $Ce^{4+}/Ln^{3+}$  separation factors ( $O/A = 0.5$ ,  $[Ln] = 7.5$  mmol  $L^{-1}$ ).

distribution of  $Ln^{3+}$  cations varies predictably with the extractant concentration as shown in equation (3), [46,49] the same was not observed in HES. To highlight this, the logarithm of  $D_{Ln}$  presented in Fig. 3A-B were plotted against that of the TOPO concentration in the HES, with the resulting graphical slope analysis presented in Figure S2. Sterically impossible slope values of 16.7 and 9.9 were obtained for  $Eu^{3+}$  and  $Lu^{3+}$  respectively at 1.0 mol  $L^{-1}$   $HNO_3$  with these values decreasing to 2.3 and 7.9 at 6.0 mol  $L^{-1}$   $HNO_3$ . Such unrealistic values and their change with the aqueous phase acidity emphasises both the difference in the two extraction regimes and the inability of slope analysis to adequately capture the extraction mechanism in these complex systems.

Unlike the trivalent  $Ln^{3+}$ , tetravalent cerium is efficiently extracted across all tested compositions.  $Ce^{4+}$  is often used as a relevant but non-radioactive analogue of tetravalent actinides, especially of  $Np^{4+}$  and  $Pu^{4+}$ , [69] which could be of interest towards the PUREX process when also considering the reported affinity of TOPO-based DES for uranyl nitrate [20]. Comparison of the distribution ratio of  $Ce^{3+}$  and  $Ce^{4+}$  with  $HNO_3$  concentration for  $x_{TOPO} = 0.5$  is presented in Figure S3 and shows a maximum separation of the tetravalent from trivalent state at 6.0 M  $HNO_3$  with  $SFCe(IV)/Ce(III) = 119.4$ . At this acid concentration,  $Ce^{4+}$  extraction is independent of the HES phase TOPO concentration as shown in Fig. 3B and Figure S2. The selectivity towards the higher valency  $Ce^{4+}$  is consistent with the greater charge density of the cation as well as possible speciation effects at higher  $HNO_3$  concentrations at which polynuclear oxo-bridged  $Ce^{4+}$  complexes of the type  $[(H_2O)_6Ce_2O(NO_3)_6]$  were reported [69–70]. Modification of  $x_{TOPO}$  can be further harnessed to improve the  $Ce^{4+}$  selectivity towards middle and heavy lanthanides at the investigated  $HNO_3$  concentration as shown in Fig. 3C. By exploiting the inefficient extraction of the trivalent lanthanides at lower  $x_{TOPO}$  compositions, an improved  $Ce^{4+}/Eu^{3+}$  and  $Ce^{4+}/Lu^{3+}$  separation factors of 195.1 and 25.3 respectively were achieved at 1.0 mol  $L^{-1}$   $HNO_3$  and  $x_{TOPO} = 0.3$  compared to the corresponding negligible values of 1.34 and 1.64 obtained for  $x_{TOPO} = 0.5$ . Interestingly, results in Fig. 3A-B show that the extraction dependency of  $Ln^{3+}$  and  $Ce^{4+}$  with the initial aqueous  $HNO_3$  concentration is reduced for lower  $x_{TOPO}$ , this being consistent with the negligible  $HNO_3$  extraction and restructuring effects for  $x_{TOPO} = 0.3$  discuss further on.

An important assumption made so far in the rationalisation of  $D_{Ln}$  trends with  $HNO_3$  concentration and initial HES composition, namely on the importance of the HES pre-organisation on the extraction, is the unvaried nature of the extracted metal complex in the HES phase. As such, the mechanism of extraction in the  $C_{10}OOH + TOPO$  HES at three TOPO molar fraction is studied using two complementary approaches aiming to detangle the respective contribution of complexation and HES phase structuration on the  $D_{Ln}$ . First, a time resolved fluorescence spectroscopy (TRFS) using  $Eu^{3+}$  as probe is carried out to determine the nature of inner sphere of the metal-solvate species. Second, the HES phase organisation after equilibration with aqueous phases of differing acidity was followed by Raman spectroscopy and small-angle X-ray

scattering (SAXS). A fixed condition of  $O/A = 0.5$  and  $T = 298$  K was applied throughout.

### 3.4. SX in TOPO + $C_{10}OOH$ – Influence of speciation

The fine structure and the relative intensities (asymmetry ratio values) of the transitions in the excitation and emission spectra of  $Eu^{3+}$  reflects the local point group symmetry of the  $Eu^{3+}$ -ligand complex whilst the number of water molecules present in the primary coordination sphere of  $Eu^{3+}$  can be gleaned from the decay profile and lifetime of its transition [71–72]. To ensure that measurable intensities were obtained for all HES phase compositions ( $x_{TOPO}$  from 0.3 to 0.5), the  $Eu^{3+}$  aqueous phase concentration was increased to 0.1 mol  $L^{-1}$  and the extraction was performed in 1.0 mol  $L^{-1}$   $HNO_3$  supplemented with 0.5 mol  $L^{-1}$   $NaNO_3$  as salting-out agent. The obtained  $D_{Eu}$  as well as the final HES-phase water content measured by Karl-Fisher titration for each  $x_{TOPO}$  are reported in Table 1. The resulting normalised excitation spectra (emission at 616.5 nm) and emission spectra (excitation at 394.0 nm) with the identified transitions [71] are presented in Fig. 4A-B whilst the TRFS of the  $Eu^{3+} {}^5D_0 \rightarrow {}^7F_2$  transition after excitation at  ${}^7F_0 \rightarrow {}^5L_6$  is shown in Fig. 4C.

The observed transitions in the absorption spectra are due to the Laporte-forbidden f-f electronic transitions of  $Eu^{3+}$ . Of interest is the increased relative intensity and red-shifting of the hypersensitive  ${}^7F_0 \rightarrow {}^5D_2$  transition in the HES phase relative to its aqueous spectrum, shown in Figure S4, suggesting the partial displacement of water molecules from the first coordination sphere of  $Eu^{3+}$ . The luminescence spectra of  $Eu^{3+}$  in the  $C_{10}OOH + TOPO$  for all molar fractions are defined by the  ${}^5D_0 \rightarrow {}^7F_J$  ( $J = 0, 1, 2, 3, 4$ ) transitions. The spectra are

Table 1

$D_{Eu}$  and HES-phase water content after extraction of  $Eu^{3+}$  ( $[Eu]_{aq,ini} = 0.1$  mol  $L^{-1}$ ) from an aqueous solution containing 1.0 mol  $L^{-1}$   $HNO_3$  and 0.5 mol  $L^{-1}$   $NaNO_3$  for three  $x_{TOPO}$ . Resulting asymmetry ratio (AR, the ratio of  $I_{616.5}/I_{591.0}$ ), luminescence lifetime ( $\tau$ ) and number of inner-sphere water molecules ( $n_{H_2O}$ ) of the extracted  $Eu^{3+}$  complex in the HES-phase.

$x_{TOPO}$	$[HNO_3]_{aq}$ (mol $L^{-1}$ )	$D_{Eu}$	$[H_2O]_{DES}$ (wt %)	AR	$\tau_{H_2O}$ (ms)	$\tau_{D_2O}$ (ms)	$n_{H_2O}$
0.3	1.0	0.28 ± 0.09	1.49 ± 0.24	5.3	1.336	1.745	0.2
0.4	1.0	3.53 ± 0.23	1.33 ± 0.19	5.4	1.510	1.785	0.1
0.5	1.0	99.9 ± 3.69	1.26 ± 0.23	5.2	1.607	1.799	0.1
0.5	6.0	0.45 ± 0.03	0.98 ± 0.16	5.9	1.328	–	–

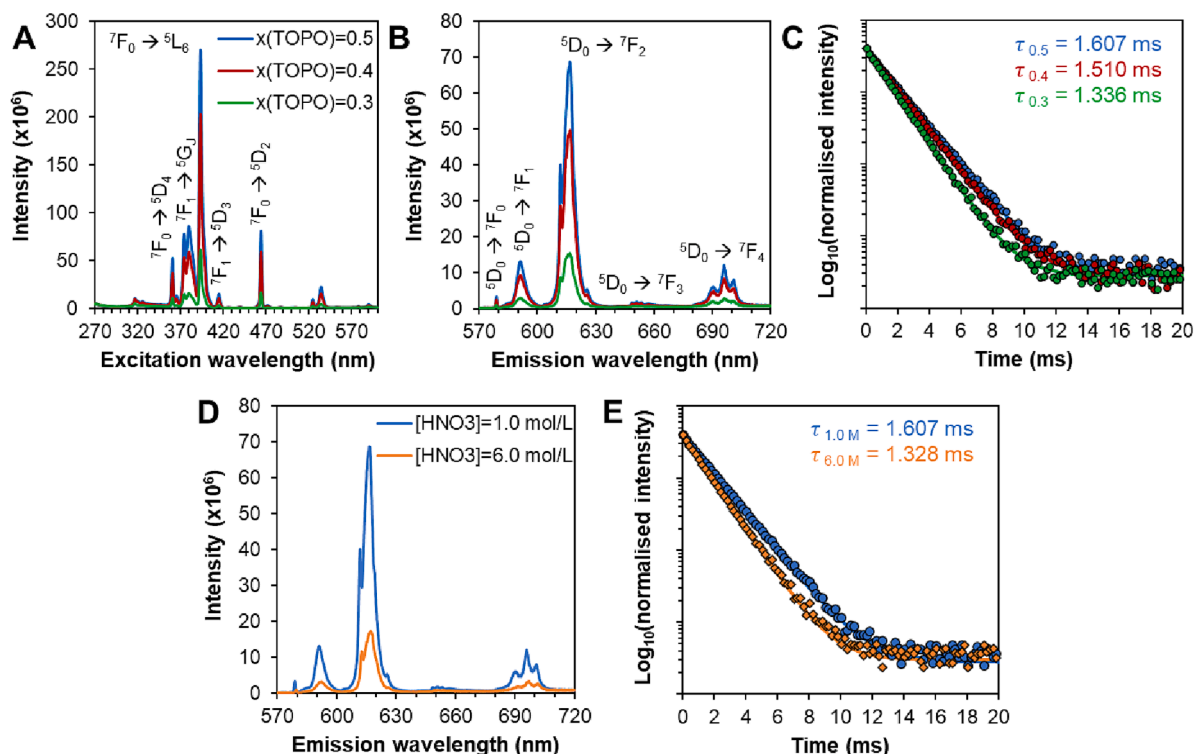


**Fig. 4.** Normalised A) excitation spectra (emission at 616.5 nm), B,D) emission spectra (excitation at 394.0 nm), and C,E) time resolved fluorescence spectroscopy of the  ${}^5D_0 \rightarrow {}^7F_2$  transition of  $\text{Eu}^{3+}$  after excitation at 394.0 nm as a function of  $x_{\text{TOPO}}$  (0.3 to 0.5) and aqueous phase  $\text{HNO}_3$  concentration (1.0 or 6.0 mol  $\text{L}^{-1}$ ) in the  $\text{C}_{10}\text{OOH} + \text{TOPO}$  HES. Lines (overlapping data points) correspond to the single exponential decay fit. Description of the HES phase composition is provided in Table 1.

dominated by the hypersensitive  ${}^5D_0 \rightarrow {}^7F_2$  transition, with an intensity approximately 5.3 times that of the  ${}^5D_0 \rightarrow {}^7F_1$  transition (see Table 1), indicative of a geometry without an inversion center [71]. Additionally, a narrow band is observable for the  ${}^5D_0 \rightarrow {}^7F_0$  transition characteristic of complexes with  $C_n$ ,  $C_{nv}$  and  $C_s$  symmetry [71]. Of the possible coordination geometries, the only ones that allow a  ${}^5D_0 \rightarrow {}^7F_0$  transition are the bicapped trigonal prism (coordination number = 8,  $C_{2v}$  symmetry) and the capped square antiprism (coordination number = 9,  $C_{4v}$  symmetry). The number of peaks in the  ${}^7F_0 \rightarrow {}^5D_0$  excitation spectrum was also previously shown to correspond to the number of distinct local environments of the  $\text{Eu}^{3+}$  cation [73]. The existence of a sole  ${}^5D_0 \rightarrow {}^7F_0$  transition for all compositions suggests that only one dominant  $\text{Eu}^{3+}$ -complex, most likely with a capped square antiprism geometry when considering the extraction results from Fig. 1, is present in the HES phase. The TRFS data for all three HES compositions in  $\text{H}_2\text{O}$  is presented in Fig. 4C whilst the same analysis in deuterated water ( $\text{D}_2\text{O}$ ) is available in Figure S5. The decay profiles were fitted with a single exponential decay function from 0.0 to 6.0 ms and the lifetime ( $\tau$ ) of the  ${}^5D_0 \rightarrow {}^7F_2$  transition are summarised in Table 1 as well as the derived number of inner-sphere water molecules ( $n_{\text{H}_2\text{O}}$ ) obtained using equation (5) [72].

$$n_{\text{H}_2\text{O}} = 1.05 \times \left( \frac{1}{\tau_{\text{H}_2\text{O}}} - \frac{1}{\tau_{\text{D}_2\text{O}}} \right) \quad (5)$$

Considering the uncertainty associated with the  $n_{\text{H}_2\text{O}}$  correlation of  $\pm 0.5$  water molecules, it appears that the first coordination shell of  $\text{Eu}^{3+}$  is dehydrated for all HES phase composition and that the co-extracted water content in Table 1 does not influence the nature of the metal ion complex. The decrease in the luminescence lifetime in  $\text{H}_2\text{O}$  as  $x_{\text{TOPO}}$  is reduced from 0.5 to 0.3 (Fig. 4C) is therefore probably due to the presence of quenching species such as water or carboxylic acid molecules in the outer-sphere of the  $\text{Eu}^{3+}$  complex. Overall, luminescence measurements confirm that  $\text{Eu}^{3+}$  is present in the same chemical environment for all HES compositions.

### 3.5. SX in TOPO + C<sub>10</sub>OOH – Influence of HES-phase composition and structure

Having ruled out speciation (for a given  $\text{Ln}^{3+}$ ) as a justification for the observed  $D_{\text{Ln}}$  trends in Figs. 1 and 3, attention is now paid to the influence of the HES phase composition and structuration on metal partitioning. In a first instance, the extraction of polar solutes, namely  $\text{HNO}_3$  and  $\text{H}_2\text{O}$ , after equilibration with aqueous phases of 1.0 and 6.0 mol  $\text{L}^{-1}$   $\text{HNO}_3$  in the absence of metal cation was determined for three HES compositions of  $x_{\text{TOPO}}$  from 0.3 to 0.5. The results are available in Table S5. Although the  $\text{HNO}_3$  and  $\text{H}_2\text{O}$  solubilities in the HES phase are moderate, conversion of these values to molar percentages, as shown in Fig. 5, indicates a drastic change in the nature of the HES phase particularly when considering their additional degrees of hydrogen-

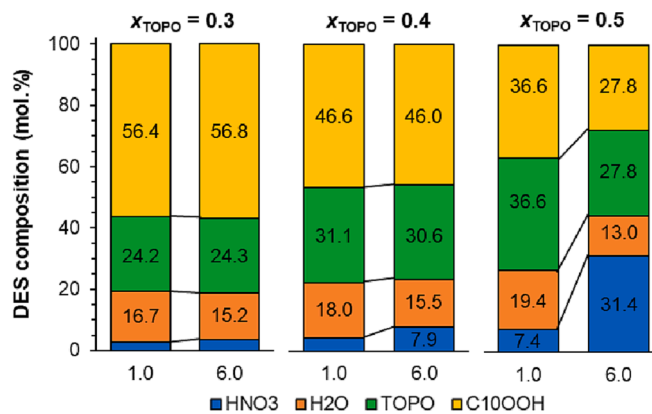


**Fig. 5.** Initial aqueous phase  $\text{HNO}_3$  concentration on the  $\text{C}_{10}\text{OOH} + \text{TOPO}$  HES phase composition at equilibrium for three  $x_{\text{TOPO}}$  values. The extracted water and acid content to the HES phase are reported in Table S5.

bonding freedom compared to  $C_{10}OOH$  and TOPO. The extraction of  $H_2O$  does not significantly vary across the tested conditions, with the measured variations in HES compositions primarily induced by  $HNO_3$  partition. Equilibrium constants ( $K$ ) of the TOPO- $HNO_3$  extraction pair in conventional SX are in the range of  $0.66 \leq \ln(K) \leq 1.28$  depending on diluting solvent, [57] reflecting the affinity of TOPO for molecular  $HNO_3$ . The extent of  $HNO_3$  partition is dependent on the initial  $x_{TOPO}$ , i. e. the  $n(TOPO):n(C_{10}OOH)$  ratio dictating the number of free TOPO ligands, and aqueous  $HNO_3$  concentration. Whilst the extraction of  $HNO_3$  varies approximately linearly with  $x_{TOPO}$  for  $1.0 \text{ mol L}^{-1}$   $HNO_3$ , it changes to an exponential relationship at  $6.0 \text{ mol L}^{-1}$   $HNO_3$ . For  $x_{TOPO} = 0.5$ , the two extraction regimes first identified in Fig. 1B, namely a “complexation dominated” one for  $[HNO_3] \leq 1.0 \text{ mol L}^{-1}$  to an “ $HNO_3$  dominated” one for  $[HNO_3] > 1.0 \text{ mol L}^{-1}$ , are clearly reflected in the  $n(HNO_3)$  to  $n(TOPO)$  ratio of Fig. 5. Within experimental error, the 1:1 ratio of  $n(HNO_3):n(TOPO)$  obtained for an initial aqueous  $HNO_3$  concentration of  $6.0 \text{ mol L}^{-1}$   $HNO_3$  suggest that TOPO( $HNO_3$ ) is now the dominant form of the ligand.

To ascertain if the change in the nature of the eutectic phase composition is reflected in its structuration and potentially on its extraction performance, the HES phase for  $x_{TOPO}$  from 0.3 to 0.5 before and after equilibration was analysed by Raman spectroscopy and SAXS. Raman analysis of the  $C_{10}OOH + TOPO$  eutectic after preparation in Fig. 6 focuses on the carboxylic region as the P = O stretch vibrations of TOPO between  $1100$  and  $1200 \text{ cm}^{-1}$  unfortunately overlaps with those of  $C_{10}OOH$  (cf Figure S6 for the full spectra between  $500$  and  $1800 \text{ cm}^{-1}$ ) [37]. The HES spectra are further compared against that of octanoic acid as it is liquid at room temperature contrary to decanoic acid, the change from  $C_{10}$  to  $C_8$  alkyl chain is not expected to impact the interpretation. The carboxylic region from  $1580$  to  $1800 \text{ cm}^{-1}$  was deconvoluted into three contributions, namely that of the carboxylic cyclic dimer at  $1660 \text{ cm}^{-1}$  and two weaker H-bond interactions at  $1716 \text{ cm}^{-1}$  and  $1734 \text{ cm}^{-1}$ .

The HES phase for  $x_{TOPO} = 0.5$  is dominated by the band at  $1716 \text{ cm}^{-1}$  assigned to the 1:1  $C_{10}OOH:TOPO$  H-bonded adduct, which gradually disappears as more  $C_{10}OOH$  is added. Although a 1 to 1 association is discussed, it is important to reiterate that this is a practical simplification as liquid HES are in a dynamic equilibrium. The emergence of a red-shifted band at  $1734 \text{ cm}^{-1}$  suggests a weakening in the individual TOPO- $HOOC_{10}$  H-bond as TOPO is included as part of H-bonded oligomeric chain network where the number of hydrogen liaisons per TOPO molecule is between one to two in accordance with previous molecular dynamic simulations [27]. The results in Fig. 6A indicate the “entrapment” of TOPO in the HES phase with decreasing  $x_{TOPO}$ , effectively raising the energetic barrier to  $Ln^{3+}$  complexation through the breakage of multiple H-bonds. The extraction of polar solutes to the HES phase ( $x_{TOPO} = 0.5$ ), namely  $H_2O$ ,  $HNO_3$ , and  $Eu^{3+}$ , also disrupt the 1:1  $C_{10}OOH:TOPO$  H-bond as shown in Fig. 6B and the resulting band dislocation relative to that in the pure HES at  $1716 \text{ cm}^{-1}$ . Despite the introduction of ionic interaction after  $Eu^{3+}$  extraction, the weakening of the HB association of  $C_{10}OOH$  is more pronounced upon  $HNO_3$  inclusion in the HES phase. The HES spectrum following equilibration with a  $6.0 \text{ mol L}^{-1}$   $HNO_3$  solution exhibits a notable band of the carboxylic dimer at  $1660 \text{ cm}^{-1}$ , confirming the liberation of  $C_{10}OOH$  due to the preferential interaction of TOPO with  $HNO_3$  and the formation of an extended H-bonded network as inferred from the COOH bands shift from  $1716 \text{ cm}^{-1}$  to  $1732 \text{ cm}^{-1}$ . The similarities between the HES phase spectra for  $x_{TOPO} = 0.3$  and  $x_{TOPO} = 0.5$  after equilibration with  $6.0 \text{ mol L}^{-1}$   $HNO_3$  suggest that the excess presence of strong H-bond donor, achieved through the variation in the HES HBD ratio or solute co-extraction, negatively affects the obtained  $D_{Ln}$  under these conditions due to the reduction in the number of weakly H-bonded TOPO ligands.

The internal liquid structure of the HES phase was further probed by SAXS to better understand the link between its self-organisation at the nanoscale and the macroscale properties described until now. SAXS relies on the difference in the scattering of X-rays due to the aggregation of

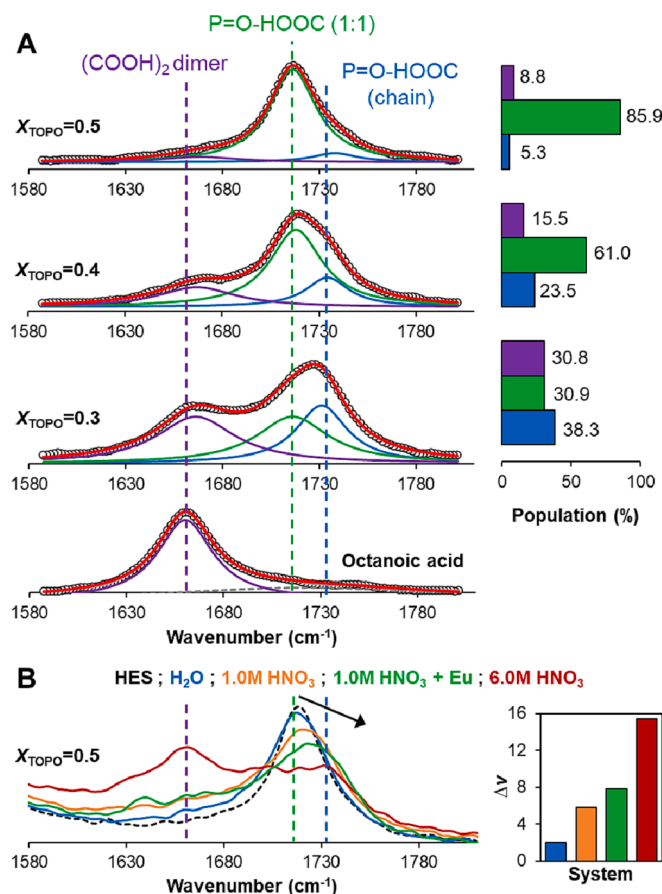


**Fig. 6.** A) Raman analysis of the  $C_{10}OOH + TOPO$  HES after preparation showing the deconvolution of the carboxylic bands and their comparison against liquid octanoic acid. Spectra were fitted using Lorentz bands after baseline subtraction (black circles – experimental data after baseline subtraction; red line – cumulative fit). B) Raman analysis of the  $C_{10}OOH + TOPO$  HES for  $x_{TOPO} = 0.5$  after equilibration with  $H_2O$ ,  $1.0$  and  $6.0 \text{ mol L}^{-1}$   $HNO_3$ , and an  $[Eu]_{aq,ini} = 0.1 \text{ mol L}^{-1}$  solution containing  $1.0 \text{ mol L}^{-1}$   $HNO_3$  and  $0.5 \text{ mol L}^{-1}$   $NaNO_3$  ( $D_{Eu}$  given in Table 1). The shift in the HES peak at  $1716 \text{ cm}^{-1}$  with the aqueous phase composition is shown in inset ( $O/A = 0.5$ ). All spectra are standardised relative to the  $CH_2$  band at  $2901 \text{ cm}^{-1}$ . (For interpretation of the references to colour in this figure legend, the reader is referred to the web version of this article.)

electron-rich molecular groups (extractant headgroups, water, acid, ions) relative to the surrounding electron-poor alkyl chains. The supramolecular organisation of the HES is rationalised based on the extensive literature addressing the liquid structure of monohydroxy alcohols with long alkyl chains such as octanol [74–75]. In such systems, a polar/apolar segregation was observed in which the presence of H-bonds bonds facilitate the transformation of small polar domains into longer H-bonded chain-like prolate clusters as illustrated in Fig. 7A [75–77]. The resulting SAXS scattering arising from intermolecular interactions is characterized by a “pre-peak” at lower  $Q$  values related to the nano-to-mesoscale structure of the H-bond network and an “adjacency peak” at higher  $Q$  values resulting from correlations between neighbouring atoms as exemplified in Fig. 7B. The pre-peak represents a correlation distance between the polar domains that are separated by the alkyl chains penetrating in each other. The distance between domains should be about  $\sim 1.5$ – $1.8$  time the average length of the alkyl chains as was reported for linear alcohols [74–75]. In the absence of information on the size and shape of these domains, an analytical description of the SAXS pattern in term of form and structure factor is complex and will represent the subject of a future work.

The SAXS profile of the HES phase with compositions corresponding

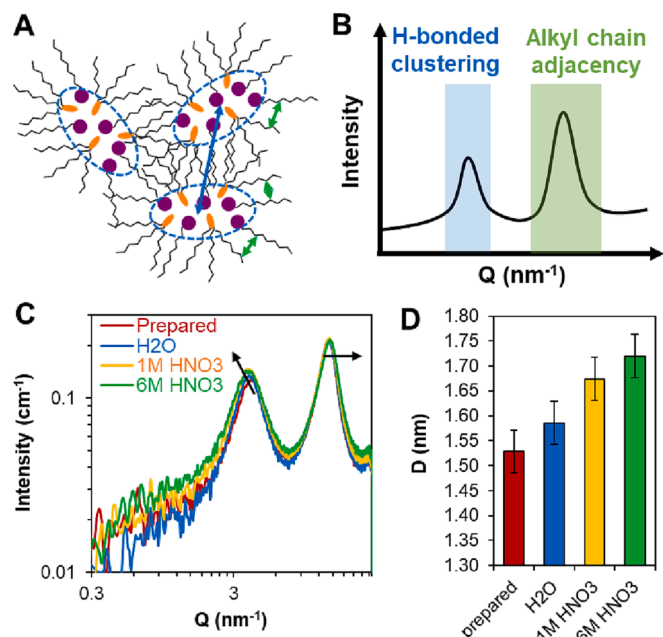


**Fig. 7.** Simplified schematic of A) a possible mixed  $C_{10}OOH + TOPO$  cluster showing the prolate-shaped polar core and B) its manifestation as peaks in the SAXS profile. C) Scattering curves of the  $C_{10}OOH + TOPO$  HES for  $x_{TOPO} = 0.5$  after preparation and equilibration with  $H_2O$ , 1.0 and 6.0 mol  $L^{-1}$   $HNO_3$ . Arrows indicate the shift in the peak position with the change in composition. D) Real space distance of the pre-peak maxima in panel C) obtained using  $D = 2\pi/Q_{max}$ , error bars correspond to the standard error.

to those in Fig. 6B and summarised in Table S5 are presented in Fig. 7C. A zoom of the peak regions is also provided in Figure S7 for greater clarity. The prepared HES displays a pre-peak centred at  $4.1 \text{ nm}^{-1}$  and a second at  $13.9 \text{ nm}^{-1}$ . A similar profile was observed in the 1:1 thymol + menthol eutectic mixture albeit with a greater pre-peak  $Q$  value of  $6.0 \text{ nm}^{-1}$ , [36] most likely due to the lower conformational flexibility of the components and poorer packing characteristic of the isopropane group preventing the formation of extended H-bonded chains. Converting the pre-peak position of the  $C_{10}OOH + TOPO$  ( $x_{TOPO} = 0.5$ ) to its real space distance given by  $D = 2\pi/Q_{max}$  gives  $1.53 \text{ nm}$ . This represents approximately 1.7 times the length of the octyl alkyl chain of TOPO in a fully trans configuration ( $\sim 0.9 \text{ nm}$ ), in line with previously suggested overlap of the aliphatic domains between clusters. The extraction of polar solutes ( $H_2O$  and  $HNO_3$ ) and their incorporation into the HES H-bond network swells the domain size as evidenced by the broadening of the pre-peak and its shift to lower  $Q$  values as the concentration of polar solutes increases after equilibration with  $H_2O$ , 1.0 mol  $L^{-1}$   $HNO_3$  and finally 6.0 mol  $L^{-1}$   $HNO_3$ . The scattering changes relative to the prepared HES are small but consistent and become more apparent when converted to the real space distance of the pre-peak maxima in Fig. 7D. The latter clearly shows the increase in the H-bonding domain distance by  $\sim 0.2 \text{ nm}$  in the HES after equilibration with 6.0 mol  $L^{-1}$   $HNO_3$  and is coherent with the inferred coordination changes by Raman of the components upon  $H_2O$  and  $HNO_3$  extraction as their smaller size allows them to intercalate between  $C_{10}OOH$  and TOPO. It is worth noting however that the pre-peak shift does not vary proportionally with the aqueous phase acidity as only small differences are observed between 1.0 and 6.0 mol  $L^{-1}$   $HNO_3$  (c.f. Figure S7). The SAXS data, regardless of the studied aqueous phase composition, does not present any low- $Q$  scattering ( $Q < 1 \text{ nm}^{-1}$ ) thereby indicating the homogeneous dispersion of the extracted solutes in the HES phase and the absence of large-scale structural heterogeneities.

Relating these observations to  $Ln^{3+}$  extraction suggests that both the polar domain size and its composition contribute to  $D_{Ln}$ . The

augmentation of the H-bond network provides a greater volume for ion solvation, lowering the barrier for extraction and yielding an initial increase in  $D_{Ln}$  for  $HNO_3$  concentrations between 0.1 and 1.0 mol  $L^{-1}$  irrespective of the  $Ln^{3+}$  cation. A similar justification was previously reported for the increase in  $Eu^{3+}$  and  $Nd^{3+}$  extraction using  $N,N'$ -dimethyl- $N,N'$ -dioctylhexylethoxymalonamide (DMDOHEMA) in heptane as the  $HNO_3$  concentration was increased to 3.0 mol  $L^{-1}$  [41–42]. However, a change in the nature of the HES polar network composition is observed from 1.0 to 6.0 mol  $L^{-1}$   $HNO_3$  at which  $n(HNO_3) \gg n(H_2O)$  (cf. Fig. 5), corresponding to a decrease in  $D_{Ln}$ . The absence of domain size restriction on  $Ln^{3+}$  extraction at greater aqueous phase acidities, i.e.  $r_{Polar \text{ domain}} > r_{Ln(NO_3)_3}$ , suggests that the relative increase in the partition of the heavy over light  $Ln^{3+}$  is attributable to the competition in TOPO coordination between  $Ln^{3+}$  and  $HNO_3$  and varies with the charge density of  $Ln^{3+}$ . Comparison of the HES for  $x_{TOPO} = 0.3$  under the same conditions as those reported for  $x_{TOPO} = 0.5$  is available in Figure S8. Contrary to that observed in Fig. 7, for  $x_{TOPO} = 0.3$  the pre-peak position, centred at  $Q = 3.7 \text{ nm}^{-1}$  in the prepared HES, is practically insensitive to the initial aqueous phase composition. The increased “rigidity” of the HES phase in the presence of excess  $C_{10}OOH$  suppresses the growth and/or elongation of the H-bonded domains, thereby preventing the formation of polar cavities with sufficient volume to accommodate extracted Ln ions. The influence of the HES composition is reflected both in its extraction performance as well as in its pre-organisation, with the latter influencing the former.

The impact of  $Ln^{3+}$  extraction on the HES phase structure was assessed by equilibrating the HES phase for  $x_{TOPO} = 0.5$  with aqueous solutions of 1.0 mol  $L^{-1}$   $HNO_3$  containing varying contents of  $Eu(NO_3)_3$  (0.1 and 0.2 mol  $L^{-1}$ ) and  $NaNO_3$  (0.5, 1.0, and 2.0 mol  $L^{-1}$ ) to yield final HES phase concentrations of 14.0, 36.3 and 75.3 g( $Eu$ )  $L^{-1}$ . The resulting SAXS profiles are presented in Fig. 8A and present an increase in the intensity with metal content due to the improved contrast of the electron-rich regions. More relevant, the diffractograms show the

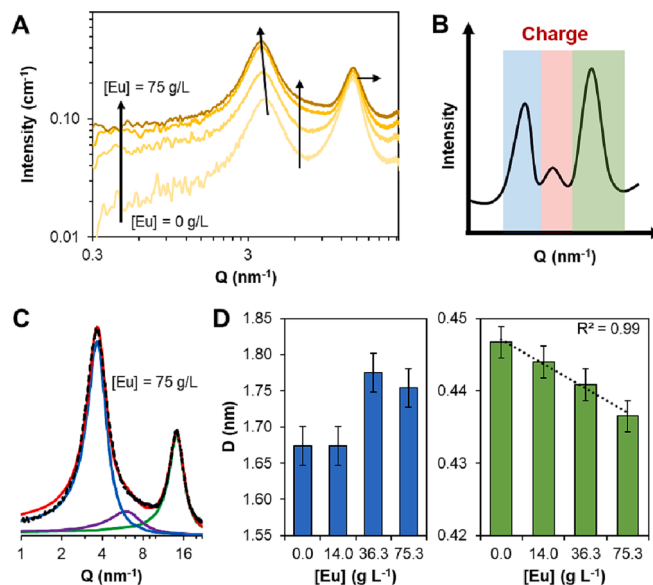


**Fig. 8.** A) Scattering curves of the  $C_{10}OOH + TOPO$  HES for  $x_{TOPO} = 0.5$  containing varying  $Eu^{3+}$  concentrations from 0.0 to 75.3 g  $L^{-1}$ . Extraction conditions:  $[HNO_3] = 1.0 \text{ mol } L^{-1}$ ;  $[Eu(NO_3)_3] = 0.1$  or  $0.2 \text{ mol } L^{-1}$ ,  $[NaNO_3] = 0.5, 1.0, \text{ and } 2.0 \text{ mol } L^{-1}$ ;  $O/A = 0.5$ . B) Simplified schematic of the charge correlation peak in the SAXS profile. C) Example deconvolution of the HES diffractogram containing 75.3 g  $L^{-1}$  of  $Eu^{3+}$  (black circles – experimental data after baseline subtraction; red line – cumulative fit). D) Real space distance of the pre-peak (blue bars) and adjacency peak (green bars) maximum as a function of the  $Eu^{3+}$  concentration, error bars correspond to the standard error. (For interpretation of the references to colour in this figure legend, the reader is referred to the web version of this article.)

emergence of a third shoulder peak at  $\sim 6.0 \text{ nm}^{-1}$  not found in the original HES spectra. The resulting pattern with three distinct peaks, illustrated in Fig. 8B and experimentally evidenced in Fig. 8C after deconvolution, is reminiscent of those observed in ionic liquids and is assigned to ion-ion correlations due the emergence of  $\text{Eu}^{3+}$  and  $\text{NO}_3^-$  charge ordering as the saturation limit of the HES is approached [78]. The introduction of electrostatic forces in the previously non-ionic HES phase results in an organisation of the aliphatic domain as shown by the linearly decreasing distance  $D$  of the adjacency peak with  $\text{Eu}^{3+}$  concentration in Fig. 8D, indicating a gradual contraction between neighbouring alkyl chains. In contrast, the domain size indicated by the pre-peak does not vary until a jump of  $\sim 0.1 \text{ nm}$  for  $[\text{Eu}] \geq 36 \text{ g L}^{-1}$  with no changes thereafter. The SAXS results indicate a restructuring of the HES phase beyond a certain  $\text{Ln}^{3+}$  concentration, with the appearance of a charge peak above the  $[\text{Eu}] \geq 36 \text{ g L}^{-1}$  threshold suggesting the formation of an intermediate ionic network [79]. It will be interesting in a future work to correlate  $\text{Eu}^{3+}$  extraction with the HES H bonding network and to determine if the transformation of the HES supramolecular structure is also related to a sudden increase in the viscosity of the phase.

### 3.6. SX in TOPO + $\text{C}_{10}\text{OOH}$ – Influence of temperature

In conventional SX, a detailed investigation of the extraction thermodynamic with temperature requires the confirmation of the constancy of the extraction reaction in the studied temperature range [80]. However, in the current HES system this entails not only correcting for the heat contributions from lanthanide extraction but also considering the extraction of  $\text{HNO}_3$  as well as accounting for the change in the HES structuration (variation in the concentration of free TOPO) due to the temperature dependency of hydrogen bonding in HES [36]. For example, it was previously shown that the  $\text{Ln}^{3+}$  partition enthalpy in the TOPO – HSCN extraction system is dependent on the total TOPO concentration [81]. As such, the potentially large cumulative uncertainties stemming from these unaccounted contributions precludes a more comprehensive study. Rather, only the gross effect of temperature on the overall extraction thermodynamics is determined by measuring the  $D_{\text{Ln}}$  as a function of temperature. The distribution of the middle ( $\text{Eu}^{3+}$ ) and heavy ( $\text{Lu}^{3+}$ ) lanthanides from a  $1.0 \text{ mol L}^{-1}$   $\text{HNO}_3$  solution were determined as a function of the temperature from 298 to 343 K and HES composition. The plotted results are presented in Fig. 9A and B and the  $D_{\text{Ln}}$  values are available in Table S4 of the ESI. To complement this, the partition of competing  $\text{HNO}_3$  was also followed under the same extraction conditions but in the absence of  $\text{Ln}^{3+}$  ions, with the resulting distribution values shown in Fig. 9C. Unfortunately, the large associated errors particularly at lower  $x_{\text{TOPO}}$  compositions prevented the accurate measurement of the lighter  $\text{La}^{3+}$  for comparison and as such was not

included. Similarly, due to the higher associated error in  $D_{\text{Eu}}$  for greater  $\text{HNO}_3$  concentrations, the same study at  $6.0 \text{ mol L}^{-1}$   $\text{HNO}_3$  was not attempted at this time.

For  $x_{\text{TOPO}} \geq 0.4$ , the decrease of the  $D_{\text{Ln}}$  values for both  $\text{Eu}^{3+}$  and  $\text{Lu}^{3+}$  with the temperature indicates an exothermic extraction process. Interestingly, an inverse  $D_{\text{Ln}}$  tendency was observed at a lower TOPO molar fraction of 0.3 for both  $\text{Ln}^{3+}$  indicative of an endothermic extraction process. The inversion from an exothermic to endothermic  $\text{Ln}^{3+}$  extraction with decreasing  $x_{\text{TOPO}}$  cannot be rationalised based on  $\text{HNO}_3$  co-extraction as similar temperature dependent  $D_{\text{HNO}_3}$  profiles were obtained for all studied HES compositions as shown in Fig. 9C. Notably, the endothermic nature of  $\text{HNO}_3$  extraction by HES in the absence of metal is contrary to that obtained using  $0.05 \text{ mol L}^{-1}$  TOPO diluted in heptane for which an exothermic extraction enthalpy of  $\Delta H = -14.6 \text{ kJ mol}^{-1}$  was reported [57]. As such, a potential explanation as to the change in  $D_{\text{Ln}}$  tendency with decreasing  $x_{\text{TOPO}}$  could be due to the greater contribution of  $\text{C}_{10}\text{OOH}$  to the extraction as linear and aromatic carboxylic and dicarboxylic acids all typically present positive enthalpies of complexation with  $\text{Ln}^{3+}$  [82–83]. The apparent extraction thermodynamic parameters, representing an amalgamation of all processes occurring in parallel with to  $\text{Ln}^{3+}$  extraction, were determined by plotting the Gibbs free energies of transfer for  $\text{Eu}^{3+}$  and  $\text{Lu}^{3+}$  as a function of temperature and  $x_{\text{TOPO}}$ , with the results presented in Figure S9. Considering the simplifying assumptions made, the corresponding calculated enthalpy and entropy values, summarised in Table 2, should be regarded on a comparative basis rather than quantitative values. Similar  $\Delta H$  and  $\Delta S$  values as in Table 2 were also obtained when using the van't Hoff formalism by plotting  $\text{Ln}(D_{\text{Ln}})$  vs.  $1/T$  ( $\text{K}^{-1}$ ) assuming that  $D_{\text{Ln}}$  is proportional to a composite-equilibrium constant for the overall extraction.

The obtained  $\Delta H$  values in HES are two to three times smaller than in the comparable traditional SX, possibly reflecting the increased energetic disadvantage when TOPO acts both as the extractant and HES phase former. In the conventional SX system composed of  $0.2 \text{ mol L}^{-1}$  TOPO in toluene and an aqueous phase of  $0.1 \text{ mol L}^{-1}$   $\text{HNO}_3$  with  $3.9 \text{ mol L}^{-1}$   $\text{NaNO}_3$ ,  $\Delta H$  remains approximately constant across the  $\text{Ln}^{3+}$  series at around  $-29.0 \text{ kJ mol}^{-1}$  until  $\text{Er(III)}$  and increases slightly for the heaviest  $\text{Ln}$  [84]. In contrast,  $\text{Lu}^{3+}$  consistently presents a more negative  $\Delta H$  value than  $\text{Eu}^{3+}$  across all HES compositions. However, the larger  $\Delta H$  is offset by a greater entropic penalty as is apparent when considering the 1.2-fold stronger extraction of  $\text{Eu}^{3+}$  relative to  $\text{Lu}^{3+}$  for  $1.0 \text{ mol L}^{-1}$   $\text{HNO}_3$  and  $x_{\text{TOPO}} = 0.5$  (Fig. 1), representing an energetic contribution of  $\Delta(\Delta G) = -RT\ln(1.2) = -0.5 \text{ kJ mol}^{-1}$ . In fact, the linear dependency of the extraction  $\Delta H$  with  $\Delta S$  as shown in Figure S10 suggests the occurrence of an enthalpy–entropy compensation for  $\text{Ln}^{3+}$  extraction from nitrate media using the TOPO +  $\text{C}_{10}\text{OOH}$  HES. A similar compensation effect was observed between  $\text{Ln}^{3+}$  and ligands containing

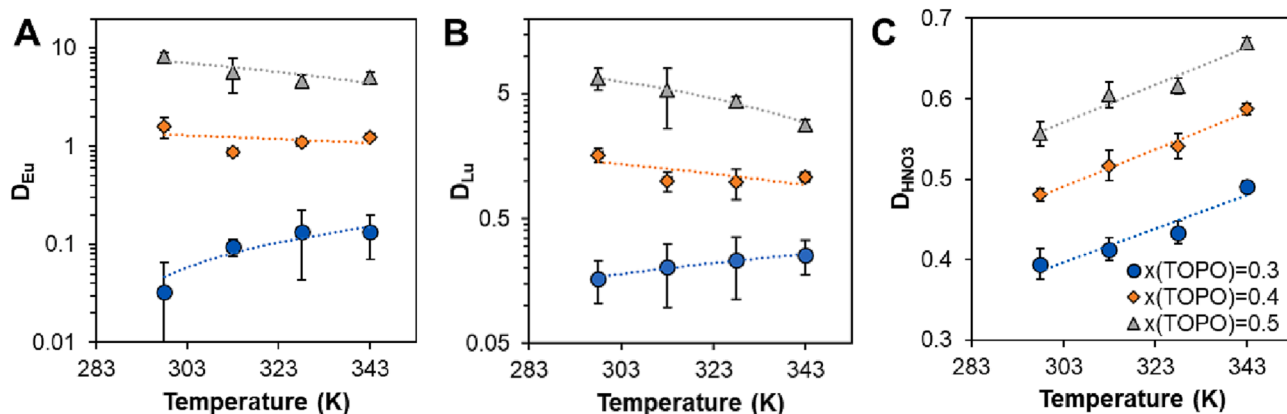


Fig. 9. Temperature and  $x_{\text{TOPO}}$  molar fraction influence on the distribution of A)  $\text{Eu}^{3+}$ , B)  $\text{Lu}^{3+}$  and C)  $\text{HNO}_3$  distribution ( $[\text{HNO}_3] = 1.0 \text{ mol L}^{-1}$ ,  $[\text{Ln}^{3+}] = 7.5 \text{ mmol L}^{-1}$  and  $\text{O/A} = 0.5$ ). All  $D$  values are available in Table S4.

**Table 2**

Values of measured values of measured entropy ( $\Delta S$ ) and enthalpy ( $\Delta H$ ) derived from the slope and intercept respectively of the curves in **Figure S7** of the ESI.

$x_{\text{TOPO}}$	Eu <sup>3+</sup>			Lu <sup>3+</sup>			HNO <sub>3</sub>		
	0.3	0.4	0.5	0.3	0.4	0.5	0.3	0.4	0.5
$\Delta H$ (kJ mol <sup>-1</sup> )	23.3	-2.5	-8.6	8.9	-6.7	-15.2	3.6	3.7	3.3
$\Delta S$ (J K <sup>-1</sup> mol <sup>-1</sup> )	51.9	-6.4	-12.4	14.0	-20.0	-35.2	-4.5	-6.3	-6.1

hard donor atoms, [80] including TOPO [85]. Differing from the enthalpy-driven nature of Ln<sup>3+</sup> extraction with TOPO [81,84] and most extractants [80] in conventional SX, entropy appears to play a more significant role in SX in HES as  $|\Delta G_{\text{R}}| \leq |-T\Delta S|$  for most  $x_{\text{TOPO}}$  and temperature combinations. As expected from the results in **Fig. 9C**, within experimental error no difference in  $\Delta H$  and  $\Delta S$  values for the apparent extraction of HNO<sub>3</sub> was observed as a function of  $x_{\text{TOPO}}$ . Whilst a more systematic and detailed thermodynamic study is required, the obtained results and their difference with traditional SX suggest the dominant role of the intermolecular HES phase interaction on the extraction that should be explicitly considered.

#### 4. Conclusions

In this work, the extraction of lanthanides from nitrate media by the non-ideal solvent composed of C<sub>10</sub>OOH + TOPO was determined as a function of the lanthanide cation selection, HES molar fraction, HNO<sub>3</sub> concentration, and temperature. Special emphasis was placed on the determination of the relationship between the HES phase structuration and the extraction performance. A compromise between maximum Ln<sup>3+</sup> loading and selectivity was observed, driven by the variation in the quantity of weakly H-bonded TOPO and the change in the configurational entropy of the mixture. A maximum distribution for all lanthanides was observed for an aqueous phase acidity of 0.5 to 1.0 mol L<sup>-1</sup> HNO<sub>3</sub> with a preference for Eu<sup>3+</sup>, resulting in a sharp break in D<sub>Ln</sub> between the adjacent Eu<sup>3+</sup> and Gd<sup>3+</sup> to yield an interesting SF<sub>Eu/Gd</sub> of 1.8. The D<sub>Ln</sub> decreased both with increased HNO<sub>3</sub> concentrations and C<sub>10</sub>OOH content. However, this decrease was more pronounced for the light and middle Ln, allowing for a change in the extraction selectivity and a SF<sub>Lu/La</sub> of 1.15 at 4.0 mol L<sup>-1</sup> HNO<sub>3</sub>. The selectivity could be further tuned through the variation in  $x_{\text{TOPO}}$  but again at the expense of the maximum achievable D<sub>Ln</sub>. Overall, the studied HES presented good D<sub>Ln</sub> values across a range of acidities and exhibited a comparable selectivity to classical SX systems using non-ionic extractants whilst eliminating the need for volatile diluents and phase modifiers. Spectroscopic and SAXS analysis indicate that the change in extraction with  $x_{\text{TOPO}}$  and/or HNO<sub>3</sub> concentration is due to the modification of the HES phase composition and organisation rather than a change in the extracted complex. All results point towards the need to explicitly consider the HES phase structuration and its compositional changes with solute co-extraction on the Ln<sup>3+</sup> extraction, which should vary based on the “deepness” (i.e. strength of intermolecular interaction) of the HES mixture. It is expected that the presented conclusions are extrapolable to other possible HES combinations presenting a non-ideal behaviour for the extraction of metal ions and polar solutes. Looking beyond the scope of this work, HES appear as promising model solvents to explore the role of H-bonding interactions in complex liquid phases and their link to SX. Further work is required to identify suitable washing and stripping solutions capable of improving on the lanthanide separation whilst regenerating the HES phase without provoking a modification of its original HBD to HBA molar ratio.

*CRedit* authorship contribution statement

**Ueslei G. Favero:** Investigation, Writing – original draft. **Nicolas Schaeffer:** Writing – original draft, Supervision, Conceptualization. **Helena Passos:** Supervision. **Kaíque A.M.L. Cruz:** Investigation.

**Duarte Ananias:** Investigation. **Sandrine Dourdain:** Investigation. **Maria C. Hespanhol:** Conceptualization, Funding acquisition, Supervision.

#### Declaration of Competing Interest

The authors declare that they have no known competing financial interests or personal relationships that could have appeared to influence the work reported in this paper.

#### Data availability

Data will be made available on request.

#### Acknowledgments

This work was partly developed within the scope of the project CICECO-Aveiro Institute of Materials, UIDB/50011/2020, UIDP/50011/2020, and LA/P/0006/2020, financed by national funds through the FCT/MCTES. This work was supported by the Instituto Nacional de Ciências e Tecnologias Analíticas Avançadas (INCTAA)/Conselho Nacional de Desenvolvimento Científico e Tecnológico (CNPq) [grant number 465768/2014-8]; Fundação de Amparo à Pesquisa do Estado de Minas Gerais (FAPEMIG) [grant number CEX-PPM-00585-17]; CNPq [grant number 305649/2021-3, 131790/2020-0]; Coordenação de Aperfeiçoamento de Pessoal de Nível Superior (CAPES)/Fundação para a Ciência e Tecnologia (FCT) [grant number 88881.309048/2018-01]; CAPES [grant number 88882.437092/2019-01].

#### Appendix A. Supplementary material

Supplementary data to this article can be found online at <https://doi.org/10.1016/j.seppur.2023.123592>.

#### References

- [1] B.K. Reck, T.E. Graedel, Challenges in metal recycling, *Science* 337 (2012) 690–695.
- [2] V. Forti, C.P. Baldé, R. Khuer, G. Bel, The global E-waste monitor 2020: Quantities, flows, and the circular economy potential, Bonn/Geneva/Rotterdam (2020).
- [3] J. Cui, L. Zhang, Metallurgical recovery of metals from electronic waste: A review, *J. Hazard. Mater.* 158 (2008) 228–256.
- [4] A.M. Wilson, P.J. Bailey, P.A. Tasker, J.R. Turkington, R.A. Grant, J.B. Love, Solvent extraction: The coordination chemistry behind extractive metallurgy, *Chem. Soc. Rev.* 43 (2013) 123–134.
- [5] F. Xie, T.A. Zhang, D. Dreisinger, F. Doyle, A critical review on solvent extraction of rare earths from aqueous solutions, *Miner. Eng.* 56 (2014) 10–28.
- [6] D.S. Sholl, R.P. Lively, Seven chemical separations to change the world, *Nature* 532 (2016) 435–437.
- [7] K.L. Nash, A Review of the basic chemistry and recent developments in trivalent F-element separations, *Solvent Extr. Ion Exch.* 11 (1993) 729–768.
- [8] J.A. Peters, K. Djanashvili, C.F.G.C. Geraldes, C. Platas-Iglesias, The chemical consequences of the gradual decrease of the ionic radius along the Ln-series, *Coord. Chem. Rev.* 406 (2020), 213146.
- [9] T. Cheisson, E.J. Schelter, Rare earth elements: Mendeleev’s bane, modern marvels, *Science* (2019) 489–493.
- [10] R.D. Shannon, Revised effective ionic radii and systematic studies of interatomic distances in halides and chalcogenides, *Acta Crystallogr. Sect. A* 32 (1976) 751–767.
- [11] A. Roca-Sabio, M. Mato-Iglesias, D. Esteban-Gómez, É. Toth, A. De Bias, C. Platas-Iglesias, T. Rodríguez-Blas, Macrocyclic receptor exhibiting unprecedented selectivity for light lanthanides, *J. Am. Chem. Soc.* 131 (2009) 3331–3341.
- [12] D. Nomizu, Y. Sasaki, M. Kaneko, M. Matsumiya, S. Katsuta, Complex formation of light and heavy lanthanides with DGA and DODA, and Its application to mutual

- separation in DGA–DOODA extraction system, *J. Radioanal. Nucl. Chem.* 331 (2022) 1483–1493.
- [13] E. Vahidi, F. Zhao, Environmental life cycle assessment on the separation of rare earth oxides through solvent extraction, *J. Environ. Manage.* 203 (2017) 255–263.
- [14] D.O. Abranches, M.A.R. Martins, L.P. Silva, N. Schaeffer, S.P. Pinho, J.A. P. Coutinho, Phenolic hydrogen bond donors in the formation of non-ionic deep eutectic solvents: The quest for type V DES, *Chem. Commun.* 55 (2019) 10253–10256.
- [15] M.A.R. Martins, S.P. Pinho, J.A.P. Coutinho, Insights into the nature of eutectic and deep eutectic mixtures, *J. Solution Chem.* 48 (2019) 962–982.
- [16] J.M. Edgecomb, E.E. Tereshatov, G. Zante, M. Boltoeva, C.M. Folden, Hydrophobic amine-based binary mixtures of active pharmaceutical and food grade ingredients: Characterization and application in indium extraction from aqueous hydrochloric acid media, *Green Chem.* 22 (2020) 7047–7058.
- [17] E.L. Byrne, R. O'Donnell, M. Gilmore, N. Artioli, J.D. Holbrey, M. Swadzba-Kwasny, Hydrophobic functional liquids based on trioctylphosphine oxide (TOPO) and carboxylic acids, *Phys. Chem. Chem. Phys.* 22 (2020) 24744–24763.
- [18] N. Schaeffer, J.H.F. Conceição, M.A.R. Martins, M.C. Neves, G. Pérez-Sánchez, J.R. B. Gomes, N. Papaiconomou, J.A.P. Coutinho, Non-ionic hydrophobic eutectics-versatile solvents for tailored metal separation and valorisation, *Green Chem.* 22 (2020) 2810–2820.
- [19] N. Schaeffer, M.A.R. Martins, C.M.S.S. Neves, S.P. Pinho, J.A.P. Coutinho, Sustainable hydrophobic terpene-based eutectic solvents for the extraction and separation of metals, *Chem. Commun.* 54 (2018) 8104–8107.
- [20] M. Gilmore, É.N. McCourt, F. Connolly, P. Nockemann, M. Swadzba-Kwasny, J. D. Holbrey, Hydrophobic deep eutectic solvents incorporating trioctylphosphine oxide: Advanced liquid extractants, *ACS Sustain. Chem. Eng.* 6 (2018) 17323–17332.
- [21] E.E. Tereshatov, M.Y. Boltoeva, C.M. Folden, First evidence of metal transfer into hydrophobic deep eutectic and low-transition-temperature mixtures: Indium extraction from hydrochloric and oxalic acids, *Green Chem.* 18 (2016) 4616–4622.
- [22] T. Hanada, M. Goto, Synergistic deep eutectic solvents for lithium extraction, *ACS Sustain. Chem. Eng.* 9 (2021) 2152–2160.
- [23] G. Almustafa, R. Sulaiman, M. Kumar, I. Adeyemi, H.A. Arafat, I. AlNashef, Boron extraction from aqueous medium using novel hydrophobic deep eutectic solvents, *Chem. Eng. J.* 395 (2020), 125173.
- [24] S. Ni, Y. Gao, G. Yu, S. Zhang, Z. Zeng, X. Sun, Tailored ternary hydrophobic deep eutectic solvents for synergistic separation of yttrium from heavy rare earth elements, *Green Chem.* 24 (2022) 7148–7161.
- [25] A.P. Abbott, G. Capper, D.L. Davies, R.K. Rasheed, V. Tambyrajah, Novel solvent properties of choline chloride/urea mixtures, *Chem. Commun.* 1 (2003) 70–71.
- [26] A.J. Peloquin, J.M. McCollum, C.D. McMillen, W.T. Pennington, Halogen bonding in dithiane/iodofluorobenzene mixtures: A new class of hydrophobic deep eutectic solvents, *Angew. Chemie Int. Ed.* 60 (2021) 22983–22989.
- [27] S.J.R. Vargas, G. Pérez-Sánchez, N. Schaeffer, J.A.P. Coutinho, Solvent extraction in extended hydrogen bonded fluids – Separation of Pt(IV) from Pd(II) using TOPO-based type V DES, *Green Chem.* 23 (2021) 4540–4550.
- [28] A. van den Bruinhorst, S. Raes, S.A. Maesara, M.C. Kroon, A.C.C. Esteves, J. Meuldijk, Hydrophobic eutectic mixtures as volatile fatty acid extractants, *Sep. Purif. Technol.* 216 (2019) 147–157.
- [29] M.J. Kaul, V. Mandella, M.L. Dietz, Systematic evaluation of hydrophobic deep eutectic solvents as alternative media for the extraction of metal ions from aqueous solution, *Talanta* 243 (2022), 123373.
- [30] D. Bourgeois, A. El Maarang, S. Dourdain, Importance of weak interactions in the formulation of organic phases for efficient liquid/liquid extraction of metals, *Curr. Opin. Colloid Interface Sci.* 46 (2020) 36–51.
- [31] M. Spadina, J.F. Dufreche, S. Pellet-Rostaing, S. Marčelja, T. Zemb, Molecular forces in liquid-liquid extraction, *Langmuir* 37 (2021) 10637–10656.
- [32] R. Motokawa, T. Kobayashi, H. Endo, J. Mu, C.D. Williams, A.J. Masters, M. R. Antonio, W.T. Heller, M. Nagao, A telescoping view of solute architectures in a complex fluid system, *ACS Cent. Sci.* 5 (2019) 85–96.
- [33] M. Spadina, K. Bohinc, T. Zemb, J.F. Dufreche, Synergistic solvent extraction is driven by entropy, *ACS Nano* 13 (2019) 13745–13758.
- [34] J. Rey, S. Dourdain, J.F. Dufreche, L. Berthon, J.M. Muller, S. Pellet-Rostaing, T. Zemb, Thermodynamic description of synergy in solvent extraction: I. enthalpy of mixing at the origin of synergistic aggregation, *Langmuir* 32 (2016) 13095–13105.
- [35] J. Rey, S. Dourdain, L. Berthon, J. Jestin, S. Pellet-Rostaing, T. Zemb, Synergy in extraction system chemistry: Combining configurational entropy, film bending, and perturbation of complexation, *Langmuir* 31 (2015) 7006–7015.
- [36] N. Schaeffer, D.O. Abranches, L.P. Silva, M.A.R. Martins, P.J. Carvalho, O. Russina, A. Triolo, L. Paccou, Y. Guinet, A. Hedou, J.A.P. Coutinho, Non-ideality in thymol + menthol type V deep eutectic solvents, *ACS Sustain. Chem. Eng.* (2021) 2203–2211.
- [37] P. Tkac, G.F. Vandegrift, G.J. Lumetta, A.V. Gelis, Study of the interaction between HDEHP and CMPO and its effect on the extraction of selected lanthanides, *Ind. Eng. Chem. Res.* 51 (2012) 10433–10444.
- [38] M.J. Servis, G.B. Stephenson, Mesostructuring in liquid-liquid extraction organic phases originating from critical points, *J. Phys. Chem. Lett.* 12 (2021) 5807–5812.
- [39] A.G. Baldwin, A.S. Ivanov, N.J. Williams, R.J. Ellis, B.A. Moyer, V.S. Bryantsev, J. C. Shafer, Outer-sphere water clusters tune the lanthanide selectivity of diglycolamides, *ACS Cent. Sci.* 4 (2018) 739–747.
- [40] D.M. Brigham, A.S. Ivanov, B.A. Moyer, L.H. Delmau, V.S. Bryantsev, R.J. Ellis, Trefoil-shaped outer-sphere ion clusters mediate lanthanide(III) ion transport with diglycolamide ligands, *J. Am. Chem. Soc.* 139 (2017) 17350–17358.
- [41] B. Qiao, T. Demars, M. Olvera De La Cruz, R.J. Ellis, How hydrogen bonds affect the growth of reverse micelles around coordinating metal ions, *J. Phys. Chem. Lett.* 5 (2014) 1440–1444.
- [42] R. Poirot, X. Le Goff, O. Diat, D. Bourgeois, D. Meyer, Metal recognition driven by weak interactions: A case study in solvent extraction, *ChemPhysChem* 17 (2016) 2112–2117.
- [43] A. Artese, S. Dourdain, N. Boubals, T. Dumas, P.L. Solari, D. Menut, L. Berthon, P. Guilbaud, S. Pellet-Rostaing, Evidence of supramolecular origin of selectivity in solvent extraction of bifunctional amidophosphonate extractants with different configurations, *Solvent Extr. Ion Exch.* 40 (2021) 431–453.
- [44] Z. Lu, S. Dourdain, S. Pellet-Rostaing, Understanding the effect of the phase modifier N-octanol on extraction, aggregation, and third-phase appearance in solvent extraction, *Langmuir* 36 (2020) 12121–12129.
- [45] J.N. Mathur, G.R. Choppin, Paraffin wax - TOPO, an extractant for actinides and lanthanides, *Solvent Extr. Ion Exch.* 16 (1997) 739–749.
- [46] B. Gupta, P. Malik, A. Deep, Solvent extraction and separation of trivalent lanthanides and yttrium using cyanex 923, *Solvent Extr. Ion Exch.* 21 (2003) 239–258.
- [47] C. Tunsu, C. Ekberg, M. Foreman, T. Retegan, Studies on the solvent extraction of rare earth metals from fluorescent lamp waste using cyanex 923, *Solvent Extr. Ion Exch.* 32 (2014) 650–668.
- [48] R. Lommelen, K. Binnemans, Hard-soft interactions in solvent extraction with basic extractants: Comparing zinc and cadmium halides, *ACS Omega* 6 (2021) 27924–27935.
- [49] A.W.G. Platt, Lanthanide phosphine oxide complexes, *Coord. Chem. Rev.* 340 (2017) 62–78.
- [50] A.C. du Preez, J.S. Preston, The solvent extraction of rare-earth metals by carboxylic acids, *Solvent Extr. Ion Exch.* 10 (2007) 207–230.
- [51] S. Dourdain, I. Hofmeister, O. Pecheur, J.F. Dufreche, R. Turgis, A. Leydier, J. Jestin, F. Testard, S. Pellet-Rostaing, T. Zemb, Synergism by coassembly at the origin of ion selectivity in liquid-liquid extraction, *Langmuir* 28 (2012) 11319–11328.
- [52] P. Dangelo, A. Zitolo, V. Migliorati, G. Chillemi, M. Duval, P. Vitorge, S. Abadie, R. Spezia, Revised ionic radii of lanthanoid(III) ions in aqueous solution, *Inorg. Chem.* 50 (2011) 4572–4579.
- [53] M. Duval, A. Ruas, L. Venaut, P. Moisy, P. Guilbaud, Molecular dynamics studies of concentrated binary aqueous solutions of lanthanide salts: Structures and exchange dynamics, *Inorg. Chem.* 49 (2010) 519–530.
- [54] T. Yaita, H. Narita, S. Suzuki, S. Tachimori, H. Motohashi, H. Shiwaku, Structural study of lanthanides(III) in aqueous nitrate and chloride solutions by EXAFS, *J. Radioanal. Nucl. Chem.* 239 (1999) 371–375.
- [55] F.J. Alguacil, F.A. López, The extraction of mineral acids by the phosphine oxide cyanex 923, *Hydrometallurgy* 42 (1996) 245–255.
- [56] J.J. Bucher, T.J. Conocchioni, E.R. Held, J.A. Labinger, B.A. Sudbury, R. M. Diamond, Extraction of HReO<sub>4</sub>, HNO<sub>3</sub>, HBr and HCl by trioctylphosphine oxide in nitrobenzene and in 1,2-dichloroethane, and hydration of the anions, *J. Inorg. Nucl. Chem.* 37 (1975) 221–227.
- [57] D.M. Petković, M.M. Kopećni, A.A. Mitrović, Solvent extraction of nitric, hydrochloric and sulfuric acid and their uranyl salts with tri-n-octylphosphine oxide, *Solvent Extr. Ion Exch.* 10 (1992) 685–696.
- [58] A. Ruas, P. Pochon, J.-P. Simonin, P. Moisy, Nitric acid: Modeling osmotic coefficients and acid-base dissociation using the BMSA theory, *Dalton Transactions* 39 (2010) 10148–10153.
- [59] J. Mu, R. Motokawa, K. Akutsu, S. Nishitsuji, A.J. Masters, A Novel microemulsion phase transition: Toward the elucidation of third-phase formation in spent nuclear fuel reprocessing, *J. Phys. Chem. B* 122 (2018) 1439–1452.
- [60] D.F. Peppard, C.A.A. Bloomquist, E.P. Horwitz, S. Lewey, G.W. Mason, Analogous actinide (III) and lanthanide (III) tetrad effects, *J. Inorg. Nucl. Chem.* 32 (1970) 339–343.
- [61] I. Persson, P. D'Angelo, S. De Panfilis, M. Sandström, Hydration of lanthanoid(III), ions in aqueous solution and crystalline hydrates studied by EXAFS spectroscopy and crystallography: The myth of the “gadolinium break”, *Chem. – A Eur. J.* 14 (2008) 3056–3066.
- [62] R.C. Shiery, J.L. Fulton, M. Balasubramanian, M.T. Nguyen, J.B. Lu, J. Li, R. Rousseau, V.A. Glezakou, D.C. Cantu, Coordination sphere of lanthanide aqua ions resolved with ab initio molecular dynamics and X-ray absorption spectroscopy, *Inorg. Chem.* 60 (2021) 3117–3130.
- [63] A. Bowden, K. Singh, A.W.G. Platt, Lanthanide nitrate complexes with triethylphosphine oxide. Solid state and solution properties, *Polyhedron* 42 (2012) 30–35.
- [64] L. Bednarczyk, S. Siekierski, Extraction of light lanthanide nitrates by tri-n-butyl phosphate, *Solvent Extr. Ion Exch.* 7 (1989) 273–287.
- [65] D.F. Peppard, W.J. Driscoll, R.J. Sironen, S. McCarty, Nonmonotonic ordering of lanthanides in tributyl phosphate-nitric acid extraction systems, *J. Inorg. Nucl. Chem.* 4 (1957) 326–333.
- [66] M.L.P. Reddy, R. Luxmi Varma, T.R. Ramamohan, S.K. Sahu, V. Chakravorty, Cyanex 923 as an extractant for trivalent lanthanides and yttrium, *Solvent Extr. Ion Exch.* 16 (1998) 795–812.
- [67] Y. Sasaki, Y. Sugo, S. Suzuki, S. Tachimori, The novel extractants, diglycolamides, for the extraction of lanthanides and actinides in HNO<sub>3</sub>-n-dodecane system, *Solvent Extr. Ion Exch.* 19 (2000) 91–103.
- [68] A. Rout, K. Binnemans, Influence of the ionic liquid cation on the solvent extraction of trivalent rare-earth ions by mixtures of cyanex 923 and ionic liquids, *Dalt. Trans.* 44 (2014) 1379–1387.
- [69] M.R. Antonio, R.J. Ellis, S.L. Estes, M.K. Bera, Structural insights into the multinuclear speciation of tetravalent cerium in the tri-n-butyl phosphate-n-

- dodecane solvent extraction system, *Phys. Chem. Chem. Phys.* 19 (2017) 21304–21316.
- [70] T.J. Demars, M.K. Bera, S. Seifert, M.R. Antonio, R.J. Ellis, Revisiting the solution structure of ceric ammonium nitrate, *Angew. Chemie Int. Ed.* 54 (2015) 7534–7538.
- [71] K. Binnemans, Interpretation of europium(III) spectra, *Coord. Chem. Rev.* 295 (2015) 1–45.
- [72] R.M. Supkowski, W.D.W. Horrocks, On the determination of the number of water molecules,  $q$ , coordinated to europium(III) ions in solution from luminescence decay lifetimes, *Inorganica Chim. Acta* 340 (2002) 44–48.
- [73] W.D.W. Horrocks, D.R. Sudnick, Time-resolved europium(III) excitation spectroscopy: A luminescence probe of metal ion binding sites, *Science* 206 (1979) 1194–1196.
- [74] R. Böhmer, C. Gainaru, R. Richert, Structure and dynamics of monohydroxy alcohols-milestones towards their microscopic understanding, 100 years after Debye, *Physics Reports*, 545, Elsevier B.V., 2014, pp. 125–195.
- [75] J.L. MacCallum, D.P. Tieleman, Structures of neat and hydrated 1-octanol from computer simulations, *J. Am. Chem. Soc.* 124 (2002) 15085–15093.
- [76] B. Qiao, K.C. Littrell, R.J. Ellis, Liquid worm-like and proto-micelles: Water solubilization in amphiphile-oil solutions, *Phys. Chem. Chem. Phys.* 20 (2018) 12908–12915.
- [77] P. Silhrén, J. Swenson, J. Mattsson, D. Bowron, A. Matic, The temperature dependent structure of liquid 1-propanol as studied by neutron diffraction and EPSR simulations, *J. Chem. Phys.* 138 (2013), 214501.
- [78] O. Russina, F. Lo Celso, N.V. Plechkova, A. Triolo, Emerging evidences of mesoscopic-scale complexity in neat ionic liquids and their mixtures, *J. Phys. Chem. Lett.* 8 (2017) 1197–1204.
- [79] M. Liu, R.D. McGillicuddy, H. Vuong, S. Tao, A.H. Slavney, M.I. Gonzalez, S.J. L. Billinge, J.A. Mason, Network-forming liquids from metal-bis(acetamide) frameworks with low melting temperatures, *J. Am. Chem. Soc.* 143 (2021) 2801–2811.
- [80] M.S. Tyumentsev, M.R.S.J. Foreman, B.M. Steenari, C. Ekberg, Temperature effect on the distribution of lanthanides(III) in the perchlorate-malonamide-methyl isobutyl ketone systems, *J. Chem. Thermodyn.* 131 (2019) 133–148.
- [81] D. Brigham, C. Badajoz, G. Cote, K.L. Nash, Extraction of trivalent lanthanides and americium by tri-*n*-octylphosphine oxide from ammonium thiocyanate media, *Solvent Extr. Ion Exch.* 29 (2011) 270–291.
- [82] G.R. Choppin, P.A. Bertrand, Y. Hasegawa, E.N. Rizkalla, Y. Hasegawa, Thermodynamics of complexation of lanthanides by benzoic and isophthalic acids, *Inorg. Chem.* 21 (1982) 3722–3724.
- [83] G.R. Choppin, A. Dadgar, E.N. Rizkalla, Thermodynamics of complexation of lanthanides by dicarboxylate ligands, *Inorg. Chem.* 25 (1986) 3581–3584.
- [84] T.S. Grimes, P.R. Zalupski, L.R. Martin, Features of the thermodynamics of trivalent lanthanide/actinide distribution reactions by tri-*n*-octylphosphine oxide and bis(2-ethylhexyl) phosphoric acid, *J. Phys. Chem. B* 118 (2014) 12725–12733.
- [85] G. Suresh, M.S. Murali, J.N. Mathur, Thermodynamics of extraction of Am(III) and Eu(III) from different anionic media with tri-*n*-octyl phosphine oxide, *Radiochim. Acta* 91 (2003) 127–134.